

Soft Matter

Accepted Manuscript

This article can be cited before page numbers have been issued, to do this please use: P. Kelkar, M. Kaboolian, C. A. Atherton, E. R. Williams, S. Lindberg and K. A. Erk, *Soft Matter*, 2025, DOI: 10.1039/D5SM00597C.



This is an Accepted Manuscript, which has been through the Royal Society of Chemistry peer review process and has been accepted for publication.

Accepted Manuscripts are published online shortly after acceptance, before technical editing, formatting and proof reading. Using this free service, authors can make their results available to the community, in citable form, before we publish the edited article. We will replace this Accepted Manuscript with the edited and formatted Advance Article as soon as it is available.

You can find more information about Accepted Manuscripts in the [Information for Authors](#).

Please note that technical editing may introduce minor changes to the text and/or graphics, which may alter content. The journal's standard [Terms & Conditions](#) and the [Ethical guidelines](#) still apply. In no event shall the Royal Society of Chemistry be held responsible for any errors or omissions in this Accepted Manuscript or any consequences arising from the use of any information it contains.

Effects of Additives on the Rheology and Phase Behavior of Lamellar-Structured Concentrated Surfactant Solutions

Parth U. Kelkar,¹ Matthew Kaboolian,¹ Cornelius A. Atherton,¹ Evan R. Williams,¹

Seth Lindberg,² and Kendra A. Erk^{1*}

¹School of Materials Engineering, Purdue University, West Lafayette, IN, 47907, USA

²Corporate Engineering, The Procter & Gamble Company, West Chester, OH, 45069 USA

ABSTRACT

Structure-property-processing relationships for model lamellar structured 70 wt.% SLE_nS solutions were developed with a combination of rheometry, cross-polarized optical microscopy, calorimetry, small angle X-ray scattering, and rheo-ultrasonic speckle velocimetry. Additives were utilized to maintain high surfactant activity, reduce bulk viscosity and simplify processing. While the bulk flow behavior of neat SLE_nS solutions was similar, the effect of some additives was sensitive to the degree of ethoxylation. Linear-chain alcohols (C₂-C₅) partitioned into inter-bilayer water layers, dehydrating surfactant headgroups and inducing lamellar-to-micellar transitions. Short-chain polyols formed higher-viscosity hexagonal and mixed phases at room temperature through hydrogen bonding with surfactant headgroups. Heating beyond the upper temperature limit weakened these interactions, resulting in low-viscosity solutions. Within the lamellar phase, common salt promoted shear-induced crystallization above the equilibrium temperature range. Propylene glycol suppressed shear-induced crystallization and promoted wall-slip under shear, forming lubrication layers near the wall. These strategies offer practical levers to tune rheology and microstructure of concentrated surfactant systems, with the datasets developed providing a foundation for future modeling. Outcomes from this study inform the sustainable design and efficient processing of concentrated surfactant-based products.

Keywords: Concentrated surfactant solutions, ternary systems, lamellar-to-micellar transitions, shear-induced crystallization, wall slip.

* Corresponding author (email: erk@purdue.edu).



INTRODUCTION

Surfactants are the primary active ingredients in consumer and industrial cleaning products, such as shampoos, laundry detergents, dishwashing liquids and hard surface cleaners.^{1,2} In recent years, there has been a growing push toward concentrated formulas - products designed with higher levels of active ingredients like surfactants and minimal water content. This marks a departure from traditional formulations, where water typically constituted most of the product volume.³ Reducing or eliminating water from a product expands the design space, enabling the inclusion of actives that are otherwise unstable or insoluble in aqueous solutions.⁴ The move toward higher activity formulas is also driven by well-established environmental and economic benefits: concentrates reduce water usage, packaging waste, lower transportation costs, and align with key sustainability goals.⁵⁻⁷ A recent life cycle analysis of three dishwashing liquids found that the most concentrated detergent (~60% active) had the lowest environmental impact across several categories, as well as the lowest water consumption.⁸

Despite these benefits, concentrates introduce significant challenges that stem from the self-assembly of surfactant molecules.⁹ As surfactant concentration increases, these systems undergo lyotropic transitions from low-viscosity, optically isotropic micellar phases to highly viscous, steady or shear birefringent liquid crystalline phases, such as hexagonal, cubic and lamellar structures.¹⁰⁻¹² Traditionally, the critical packing parameter (CPP) has provided a robust framework to model these transitions.¹³ Although the more concentrated lamellar phase has a lower apparent steady shear viscosity (~10-20 Pa s at 20 °C, 1 s⁻¹) than the less concentrated hexagonal phase (~100 Pa s at 20 °C, 1 s⁻¹),^{14,15} both exhibit yield and non-Newtonian flow behaviors and characteristic of highly ordered¹⁶ liquid crystalline assemblies. These properties complicate a range of manufacturing operations starting from the unloading of raw feedstocks



from delivery vehicles such as trucks and railcars. They also lead to difficulties in downstream processes like pumping, mixing, and bottling, as well as in meeting consumer-relevant performance criteria like dissolution in water.^{17–19} A shear rate of 1 s^{-1} is frequently used as an industrial benchmark, as it is above low-shear torque limits²⁰ and below the onset of inertial and turbulent effects.^{21,22} Numerically, viscosity below 1 Pa s at this shear rate is considered acceptable for reliable pouring and pumping. Formulating systems with high surfactant activity while maintaining low viscosity continues to be a central challenge in the development of next-generation consumer cleaning products.

Differences in rheological behavior across liquid crystalline phases have important implications for process design. Hexagonal phases, composed of cylindrical surfactant micelles packed into a hexagonal array are generally avoided due to poor responsiveness to applied shear forces and temperature.¹⁵ Their inadvertent formation during manufacturing can cause pipe blockage, damage equipment, and lead to substantial economic losses.²³ In contrast, lamellar phases, comprising stacked surfactant bilayers separated by water layers, are used as high-activity feedstocks that can be more readily processed into concentrated surfactant-based products.^{14,15,24–}

26

The rheological behavior of lamellar systems, particularly highly concentrated lamellar-structured solutions, has been the focus of growing attention in recent years, with studies examining their response to temperature and applied shear across various surfactant chemistries. These trends have been reviewed by Berni *et al.*²⁷ and studied more recently by Kelkar *et al.*²⁸ Lamellar-structured anionic sodium lauryl ether sulfate (SLE_nS), where ‘n’ denotes the degree of ethoxylation, at concentrations near 70 wt.% surfactant in water has emerged as a model industrial feedstock due to its widespread use across product categories and commercial availability at scale.



In contrast to sodium dodecyl sulfate (SDS),²⁹ it forms stable, highly concentrated lamellar phases at room temperature. However, while concentrated SLE_nS systems provide a versatile processing platform, their response to formulation-relevant additives remains poorly understood. This study investigates the effect of additives on the structure and rheology of concentrated lamellar SLE_nS solutions. To address persistent challenges, trajectories through complex phase spaces were developed to reduce viscosity and improve the processability of high-active model feedstocks used in consumer cleaning products.



BACKGROUND

Sodium lauryl ether sulfate (SLE_nS) is a key surfactant across the personal cleansing and fabric care business, and recent studies have increasingly focused on its aqueous lamellar phase. Caicedo-Casso *et al.* mapped the concentration dependent (20-70 wt.%) room temperature phase behavior of SLE_1S -water and identified a lamellar phase from 60-70 wt.% surfactant. The flow behavior was characterized by shear rheometry and the presence of flow instabilities such as wall slip and plug flow were monitored with rheo-ultrasonic speckle velocimetry.¹⁵ A similar study by Castaldo *et al.* investigated the effects of surfactant concentration on dissolution, phase behavior, and rheology. Although the degree of ethoxylation was not specified, the presence of a cubic (V_1) phase suggests that the system studied was SLE_3S -water.³⁰ Experimental phases reported by Caicedo-Casso *et al.* were further validated by Hendrikse *et al.* using dissipative particle dynamics and molecular dynamics.^{31,32} Kelkar *et al.* explored the rheological and microstructural changes in neat 70 wt.% SLE_1S solutions at low-temperatures and reported shear-induced crystallization effects on the complex viscosity. Ferraro *et al.* developed a temperature-concentration phase diagram (30-60 °C) of the SLE_3S -water system.^{33,34} Their findings emphasized that molecular polydispersity within SLE_3S and SLE_1S , particularly in alkyl tail length, degrees of ethoxylation, sulfation and sulfonation, common in industrial-grade feedstocks,³⁵ could strongly influence phase and flow behavior.

Despite the growing body of work, most published studies remain focused on the bulk behavior of binary SLE_nS -water systems, whereas real-world products including simplified, essential-ingredient formulas are rarely that simple. Even the simplest commercial formulations contain additives that are used to modify viscosity, aid processing, or enhance stability and performance.³⁶ Along with traditionally recognized processing parameters (e.g., equipment type,



applied shear, pressure, and temperature ramps), the order and timing of additive incorporation can significantly affect material behavior. This represents another lever in the engineer's toolbox. For example, the 4-P+ process demonstrates how changing the order of addition, to post-adding polyols, polymers, preservatives, and perfumes as a premix in the aqueous phase can accelerate processing and improve stability.³⁷ While it may be desirable to understand the impact of every ingredient in a multicomponent formulation, this is rarely practical.

Adding a single ingredient to a surfactant-water feedstock transforms it into a ternary system. Unlike binary diagrams, ternary phase diagrams have historically been far more difficult to interpret, due in part to ambiguity in additive positioning and the tendency of systems near multiphase boundaries to undergo tie line hopping.³⁸ Despite these challenges, the breadth and depth of ternary phase science is remarkably rich. Foundational work by McBain and Elford³⁹ and Ekwall^{40,41} on ionic surfactant-water-additive systems, laid the groundwork for understanding additive effects on phase behavior. Initial studies examined potassium oleate-water-potassium chloride systems, followed by sodium octanoate-water-decanol. For more detailed discussions of ternary phase diagrams across ionic, nonionic, and zwitterionic systems the reader is referred to reviews by Lisi and Milioto,⁴² Laughlin *et al.*,⁴³ Khan,⁴⁴ Holmberg *et al.*,⁴⁵ Wennerström,⁴⁶ and Tucker.⁴⁷ While not intended to be exhaustive, significant historical investigations^{48–61} and more recent studies by Akter *et al.*,⁶² Baruah *et al.*,⁶³ Zhong *et al.*,⁶⁴ and Honaryar *et al.*⁶⁵, into alcohol, electrolyte, co-surfactant and polymer induced transitions illustrate both the evolution and enduring complexity of ternary surfactant systems.

Within this broader body of work, a smaller subset of studies has explored the effects of additives on the structural and rheological behavior of lamellar phases. Work by Murthy and Kaler and Montalvo *et al.* extensively characterized the cetyltrimethylammonium bromide (CTAB)-



water system. The effects of alcohol tail length on the temperature dependent lamellar-to-isotropic phase transition,⁶⁶ and benzyl alcohol on the rheology were investigated.⁶⁷ Roux *et al.* worked with lamellar phases of the SDS-water-pentanol and dodecanol systems to study the role of membrane flexibility on undulation interactions between membranes.⁵² The stability of lamellar phases as a function of inter- and intra-bilayer interactions in three anionic, cationic and non-ionic surfactant-water-propylene glycol systems were further investigated by Martino and Kaler.⁶⁸ Yang *et al.* used small-angle X-ray scattering to study the extent to which cyclohexane and benzene penetrated into the lamellar phase of the anionic surfactant dihydrogenated tallowalkyl dimethyl ammonium chloride (DHTDMAC).⁶⁹ Goncalves *et al.* focused on the effect of several additives on the lamellar gel phase (L_β) to more classical L_α phase transition for double-chain cationic surfactants dioctadecyldimethylammonium chloride (DODAC) and dioctadecyldimethylammonium bromide (DODAB).^{70–72} Polymer-surfactant interactions in liquid crystals were reviewed by Piculell⁷³ and further experimentally investigated for SDS and CTAB-water-polyvinylpyrrolidone (PVP) by Cukurcent and Masalci.⁷⁴

Despite its industrial relevance, the literature on ternary concentrated lamellar-structured SLE_nS systems is extremely limited. Khosharay *et al.*,⁷⁵ Choi *et al.*,⁷⁶ Pleines *et al.*,⁷⁷ Parker and Fieber⁷⁸ and Panoukidou *et al.*⁷⁹ reported additive driven changes in micellization, wormy micelle contour length and the salt curve in dilute solutions. Caicedo-Casso *et al.*¹⁵ used common salt (NaCl) to form and characterize lamellar phases with 40 wt.% SLE₁S while Kelkar *et al.* studied the effect of added NaCl on radial dissolution of feedstock lamellar pastes (70 wt.% SLE₁S).¹⁸

The goal of this experimental study was to develop material relationships between industrially relevant additives (alcohols, acetates, short-chain aliphatic polyols, hydrotropes and desiccants) and concentrated (70 wt.%) lamellar structured aqueous SLE_nS solutions. The bulk



behavior of 70 wt.% SLE₁S, SLE₂S, and SLE₃S was first characterized to establish structural and rheological baselines across degrees of ethoxylation and manufacturers. Three distinct processing strategies were developed to achieve high surfactant activity while reducing viscosity. In the first approach, short-chain linear alcohols induced lamellar-to-micellar transitions at room temperature. The second strategy used propylene glycol, glycerin, and 1,3-propanediol to drive lamellar-to-hexagonal or mixed-phase transitions, with elevated temperature enabling access to lower-viscosity zones. The third approach focused on processing within the lamellar regime, examining how propylene glycol and NaCl affected the microstructure, shear-induced crystallization, and the formation and evolution of flow instabilities like wall slip and plug flow.

Based on the initial baseline comparisons, SLE₃S was selected for the first two approaches, while SLE₁S was used for the third. Structural and rheological responses across all three strategies were characterized using a combination of shear and oscillatory rheometry, static and dynamic cross-polarized optical microscopy, small-angle X-ray scattering (SAXS), differential scanning calorimetry (DSC), and rheo-ultrasound speckle velocimetry (rheo-USV). Structure-property-processing relationships developed here provide a platform for rational formulation design, enabling control over phase behavior and rheology of concentrated surfactant systems.



184 EXPERIMENTAL SECTION

185 **Materials.** Molecular structures of all surfactants and additives are presented in
186 **Supplementary Figure S1.**

187 **Surfactants.** Lamellar-structured concentrated 70 wt.% aqueous solutions of sodium
188 lauryl ether sulfate (SLE_nS) - SLE₁S (STEOL[®] CS-170 UB), SLE₂S (STEOL[®] CS-270 Plus), and
189 SLE₃S (STEOL[®] CS-370) were all obtained from the Stepan Company, and an industrial-grade 70
190 wt.% SLE₃S paste (Kopacol[®] N70 LS ReNu Ultra) was supplied by the Procter & Gamble
191 Company. All surfactants were used as received. The SLE_nS samples consisted of a homologous
192 mixture of alkyl chains averaging 12 carbon atoms (ranging from C₁₀ to C₁₆), with n corresponding
193 to the average number of ethylene oxide (EO) units; for example, SLE₃S has an average of three
194 ethoxy groups. Bulk rheological, thermal and phase characterization of feedstock SLE₁S, SLE₂S,
195 and SLE₃S solutions (**Supplemental Figure S2**) revealed only minor differences in lamellar d-
196 spacing due to EO chain length. SLE₁S (STEOL[®] CS-170 UB) and SLE₃S (Kopacol N70 LS ReNu
197 Ultra) were used for all experiments with additives.

198 **Additives.** All additives were used without further purification. Short to medium-chain
199 alcohols - ethanol (anhydrous, 200 proof, >99.5%), isopropyl alcohol (IPA) (≥99.0%), 1-butanol
200 (99.8%), 1-pentanol (≥99%), and 1-hexanol (98%) were purchased from Sigma-Aldrich[®], as were
201 methyl acetate (≥99%), ethyl acetate (≥99.5%), propylene glycol (≥99.5%), 1,3-propanediol
202 (98%), sodium chloride (NaCl) (≥99.0%), and sodium xylenesulfonate (SXS) (≥90%). Longer-
203 chain alcohols, 1-octanol and 1-decanol (both 98%), were sourced from Alfa Aesar (now Thermo
204 Scientific chemicals), while 1-dodecanol (98%) was obtained from Sigma-Aldrich Fine Chemicals
205 (SAFC). Glycerin was supplied by the Procter & Gamble Company.



Sample Preparation. The procedures described below are based on methodologies previously established by Caicedo-Casso *et al.*¹⁵ and Kelkar *et al.*¹⁸ All samples were prepared at room temperature in 20 g batches in glass vials by mixing the appropriate amount of additive with the lamellar paste. Liquid additives were incorporated at concentrations of 1%, 2.5%, 5%, 10%, 15%, and 20% by weight, while NaCl and SXS were added at 0.5%, 1%, 2%, 2.5%, 5%, and 10% by weight. All percentages were calculated based on the total mass of the surfactant and water mixture. For all ternary mixtures, the SLE_nS:water ratio was held constant at 2.333, which resulted in final compositions (wt.%) that varied with additive loading. For example, 2.5%, 10%, and 20% added additive yielded surfactant(S):water(W):additive(A) compositions of approximately 68.3(S):29.3(W):2.4(A), 63.6(S):27.3(W):9.1(A), and 58.3(S):25(W):16.7(A) respectively.

Equilibration times ranged from a minimum of 2 days to up to 7 days, with longer durations required for samples with NaCl or SXS. SLE₁S solutions were placed on a hot plate at approximately 35 °C, sealed with Parafilm® to minimize evaporation, and gently stirred at 24-hour intervals. Samples with SLE₃S were initially equilibrated in an industrial oven at the same temperature, also sealed with Parafilm® and subjected to the same stirring schedule. Sample homogeneity was assessed through direct visual inspection. Following equilibration, all SLE₃S + additive specimens were subjected to a thermal screening to assess susceptibility to temperature dependent phase transitions. Samples were kept at 45 °C for 48 h and then at 75 °C for an additional 48 h in a convection oven, with Parafilm® seal maintained throughout. A protorheological approach⁸⁰ was used to assess flow behavior via vial inversion and selected samples with lower apparent viscosities compared to the neat lamellar baseline were analyzed further.

Ultrasound speckle velocimetry (USV) measurements required seeding each sample with an ultrasonic contrast agent to enable velocity profile acquisition. The methodology was adapted



from established protocols by Bice,⁸¹ Caicedo-Casso *et al.*¹⁵ and Manneville *et al.*⁸² Hollow glass spheres (Sigma-Aldrich) with an average diameter of 11 μm and a density of $1.1 \text{ g}\cdot\text{cm}^{-3}$ were used. The total sample volume used for measurement was approximately 20 g and the concentration of these tracers was adjusted based on the sample type: micellar solutions (STEPANOL[®] WA-EXTRA - Stepan Company) used for calibration were seeded with 1 wt.% glass spheres, while liquid crystalline (lamellar and hexagonal) specimens contained approximately 0.3 wt.%. These concentrations were sufficiently low to assume that the particles followed the flow as Lagrangian tracers. Micellar samples were sonicated for approximately 10 minutes to ensure uniform dispersion of the tracer particles and were used immediately afterward. In contrast, liquid crystalline specimens were gently mixed by hand, degassed in a vacuum oven to eliminate entrained air bubbles, and likewise used immediately following preparation.

Methods. All experiments were conducted at Purdue University and the Corporate Engineering Technology Laboratories (CETL) of The Procter & Gamble Company. Sample transport between the two facilities was minimized to reduce handling variability. When necessary, most samples were first allowed to fully equilibrate at their site of preparation and subsequently rested for at least 24 hours upon arrival before being used in experiments.

Basic Rheometry. Rheometry experiments used to measure bulk material behavior under steady and oscillatory flow, were performed using two instruments. At Purdue University, an Anton Paar MCR 702 Modular Compact Rheometer equipped with a CC10 concentric cylinder fixture (bob diameter = 10.0 mm, bob length = 14.9 mm, measurement gap = 0.422 mm) and Peltier temperature control was used. At Procter & Gamble, experiments were performed on a TA Instruments DHR-2 rheometer using a 40 mm, 2° cone-and-plate fixture with Peltier control. For temperature ramp comparisons, a DIN CC27.9 mm cup-and-bob fixture (bob diameter = 27.99



mm, measurement gap = 1.071 mm) was also used. No measurable evaporation effects were observed within the timescale of the experiments, and the cone geometry was selected to minimize sample volume. The specific fixture used for each dataset is noted in the corresponding figure.

All measurements were performed using fresh specimens from the same surfactant solution batch, conducted under steady-state conditions,²⁸ and repeated in triplicate; representative datasets are reported. Experimental protocols used in this study are similar to those previously used by Caicedo-Casso *et al.*¹⁵ and Kelkar *et al.*²⁸ To ensure consistent shear history, samples were pre-sheared at 5 s⁻¹ for 1 minute and rested for 2 minutes prior to testing. Rate controlled forward (0.1 - 100 s⁻¹) flow sweep experiments were performed (30 s/point, 10 points per decade, $\pm 5\%$ uncertainty on the DHR-2 and 7 s/point, 20 points per decade on MCR 702). The magnitude of applied oscillations during oscillatory measurements (strain amplitude, $\gamma_0 = 0.1\%$ and angular frequency, $\omega = 10$ rad/s) was within the linear viscoelastic range (LVER) of the samples.²⁸ Unless specified otherwise, the temperature was changed at 1 °C/min, with an uncertainty of ± 0.1 °C. To ensure reproducibility, rheometry experiments on selected samples were performed across multiple instruments and geometries. Rheological trends were consistent across cone-and-plate and concentric cylinder fixtures, as confirmed by flow curve and temperature ramp data (Supplementary Figure S3).

Advanced Rheo-Ultrasonic Speckle Velocimetry (rheo-USV). USV is a one-dimensional velocity profiling technique that tracks the motion of contrast agents within a deforming specimen using high-frequency backscattered ultrasound. Measurements were performed at Purdue University using a custom-built USV system developed in collaboration with Sébastien Manneville⁸², coupled to an Anton Paar MCR 302 rheometer and a concentric cylinder cell (48 mm rotor, 0.83 mm gap) fabricated from polymethyl methacrylate. The cell and transducer



were immersed in a temperature-controlled water bath to ensure uniform temperature and facilitate acoustic transmission. The USV system has a spatial resolution of $\sim 42\ \mu\text{m}$, a temporal resolution ranging from 0.1 to 100 s and operates over a shear rate range of 0.2 to $200\ \text{s}^{-1}$. The physical configuration and full experimental procedure closely follow those reported previously by Caicedo-Casso *et al.*¹⁵ and Bice.⁸¹

USV was conducted during shear-startup experiments. For each specimen, three decreasing shear rates were applied sequentially, each preceded by a corresponding pre-shear: $100\ \text{s}^{-1}$ before $70\ \text{s}^{-1}$, $10\ \text{s}^{-1}$ before $7\ \text{s}^{-1}$, and $1\ \text{s}^{-1}$ before $0.7\ \text{s}^{-1}$. Pre-shear durations were at least 20 seconds, and velocimetry data were collected after a minimum of 30 seconds of shearing to ensure steady-state behavior. Geometrical calibration of the instrument and simple shear velocity profile of a Newtonian micellar solution is shown in **Supplementary Figure S4**. All experiments were conducted at $22\ ^\circ\text{C}$.

X-ray Scattering. Small-angle X-ray scattering (SAXS) and wide-angle X-ray scattering (WAXS) measurements were conducted using an Anton Paar SAXSPPOINT 2.0 system equipped with a Cu- α X-ray source and an Eiger detector. These techniques were used to probe nanoscale structural features: d-spacing and phase identification based on characteristic scattering patterns. High-viscosity liquid crystalline samples were loaded into the Anton Paar PasteCell N fixture with polycarbonate film windows and held inside a temperature-controlled TCStage 150. Low-viscosity samples were loaded into TCStage-compatible quartz cuvettes. Static phase characterization was carried out at $25\ ^\circ\text{C}$ on key compositions including lamellar feedstocks with and without additives. Each measurement comprised three 2-minute exposures at sample-detector distances of 825 mm (SAXS) and 365 mm (WAXS).



For thermal phase change studies, samples were cooled from ambient to 20 °C at 1 °C/min and equilibrated for 2 minutes. They were then heated to target temperatures. Neat Kopacol SLE₃S was analyzed using the same protocol with sequential heating to match the range used for ternary systems of interest. At each temperature, samples were equilibrated for 2 minutes before exposure. The three-frame averaged two-dimensional scattering frames were reduced using Anton Paar's SAXSAnalysis software. One-dimensional, empty-cell-subtracted transmittance-normalized patterns were analyzed for characteristic peak structures, sizes, and positions.

Dynamic Scanning Calorimetry (DSC). All experiments were performed using a TA Instruments Q2000 DSC and hermetically sealed Tzero aluminum pans and lids. DSC was used to measure heat flow during thermal phase transitions. Unless specified otherwise, the temperature was changed at a rate of 1 °C/min.

Static Cross-Polarized Optical Microscopy and Shear-Cell Visualization. Static cross-polarized images were captured using a Keyence VHX-F series microscope equipped with a Dual-Objective VH-ZST Zoom Lens (magnification range 20x to 2000x) with polarizers. Qualitative phase identification was based on the work of Rosevear.¹⁰ For in-situ temperature ramping, a digitally controlled Linkam Peltier stage was mounted on the microscope. The initial and end temperatures, as well as the ramp speeds, were pre-programmed. Small volumes (~0.2 ml) of sample were carefully put on a glass slide, followed by 100 µm thick spacers and a cover slip.

Microstructural evolution with applied shear forces was captured using a CSS450 optical shearing system (Linkam Scientific, Tadworth UK). This is a parallel plate cell with quartz plates and a viewing window located at 7.5 mm off center; the gap and rotational velocity are electronically controlled with the Linksys32 software. The vertical gap was set to 75 µm. The stage was mounted on a Motic upright microscope (BA410E) with 5x LM Plan lens (NA 0.13) and 20x



lens (NA 0.4). Images were acquired using a FLIR Blackfly 5 MP C-mount, color, USB camera through the FLIR Spinview software. Approximately 0.2 mL of sample was deposited at the center of the shear cell stage using a syringe, and the lid was carefully secured. The shear rate was increased stepwise from 0.1 s⁻¹, 1 s⁻¹, 10 s⁻¹ with 5 s rest periods between each 30 s step. Images were collected every 250 milliseconds and stitched together.

Data Analysis. Experimental data was fitted to theoretical models using Origin 2022 (OriginLab).

RESULTS AND DISCUSSION

Three processing strategies were developed to modify phase behavior and rheology in high-active surfactant pastes (Figure 1): (1) lamellar-to-micellar transitions at room temperature, (2) lamellar-to-hexagonal or mixed-phase transition followed by heating to approach the upper temperature limit, and (3) effects of additives within the lamellar phase. In ternary surfactant-water-additive systems at constant temperature and pressure, the Gibbs phase rule limits coexistence to three phases.^{83–85} Multiple two- and three-phase regions exist in a full diagram, and the law of alternates requires transitions between single-phase regions to pass through at least one two-phase region.¹¹ Fixing the surfactant-to-water ratio constrains the accessible phase space and excludes certain transitions⁸⁶ and isolates the effect of additives on the lamellar phase.

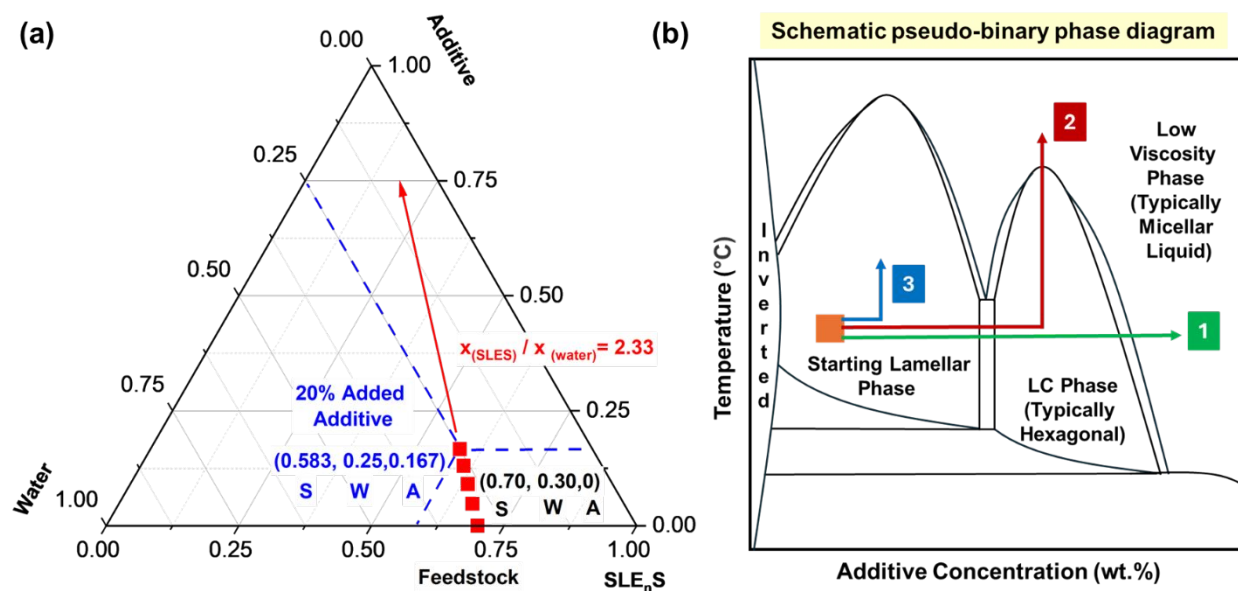


Figure 1. (a) Ternary diagram showing feedstock lamellar concentration, constant surfactant/water ratio trajectories and effective surfactant(S) : water(W) : additive(A) composition with 20 wt.% added additive, and (b) simplified, schematic pseudo-binary diagram



illustrating the three experimental approaches used in this study. Adapted from Laughlin¹¹ and Yamashita.⁸⁷

Approach 1: Lamellar to micellar transitions. Short-chain linear alcohols were effective at disrupting the lamellar structure. With increasing ethanol (Figure 2(a)) and IPA (Figure 2(b)) concentration, the shear thinning behavior characteristic of the highly viscous lamellar phase transitioned to a high-shear rate low-viscosity Newtonian plateau at the highest added concentration.¹⁵ Above 15 wt.%, both ethanol and IPA induced a lamellar-to-micellar transition causing a decrease in viscosity. As seen in Figure 3 (f) – (h), birefringent, disordered lamellar phases were dispersed in an optically dark micellar background. These domains are readily homogenized even at low shear rates, resulting in a Newtonian plateau. This transition was also confirmed by SAXS (**Supplementary Figure S5**). As ethanol concentration increased, the lamellar d-spacing decreased from $44.6 \pm 0.4 \text{ \AA}$ for neat 70 wt.% SLE₃S to $40.3 \pm 0.3 \text{ \AA}$ at 10 wt.% ethanol, with a corresponding weakening of the lamellar structure. At 20 wt.% ethanol, the system had a micellar separation distance of $37.4 \pm 2.9 \text{ \AA}$. At a fixed additive concentration (10 wt.%), increasing alcohol chain length progressively increased the 1 s^{-1} viscosity - $\sim 11 \text{ Pa s}$ (ethanol), $\sim 12 \text{ Pa s}$ (IPA), $\sim 17 \text{ Pa s}$ (butanol), $\sim 22 \text{ Pa s}$ (pentanol), $\sim 26 \text{ Pa s}$ (hexanol), 30 Pa s (decanol) and $\sim 35 \text{ Pa s}$ (dodecanol) (Figure 2 (c)).

Ethanol and other short-chain, water-soluble alcohols (C₂-C₅) selectively partition into the water layers between surfactant bilayers and compete with water for interaction sites at the surfactant headgroup interface.^{88–90} This disruption in local hydrogen bonding and apparent dehydration⁹¹ of the hydration layer around SLE₃S headgroups decreases the effective headgroup area. As the hydrophobic-to-hydrophilic volume ratio increases, the CPP changes and results in a lamellar-to-micellar transition.¹³ Although ethanol strengthens hydrogen bonding in bulk water,⁹²



this behavior is altered in liquid crystals: in lamellar systems, ethanol displaces interfacial water and reduces water layer thickness, leading to a measurable decrease in d-spacing, as observed through SAXS measurements.

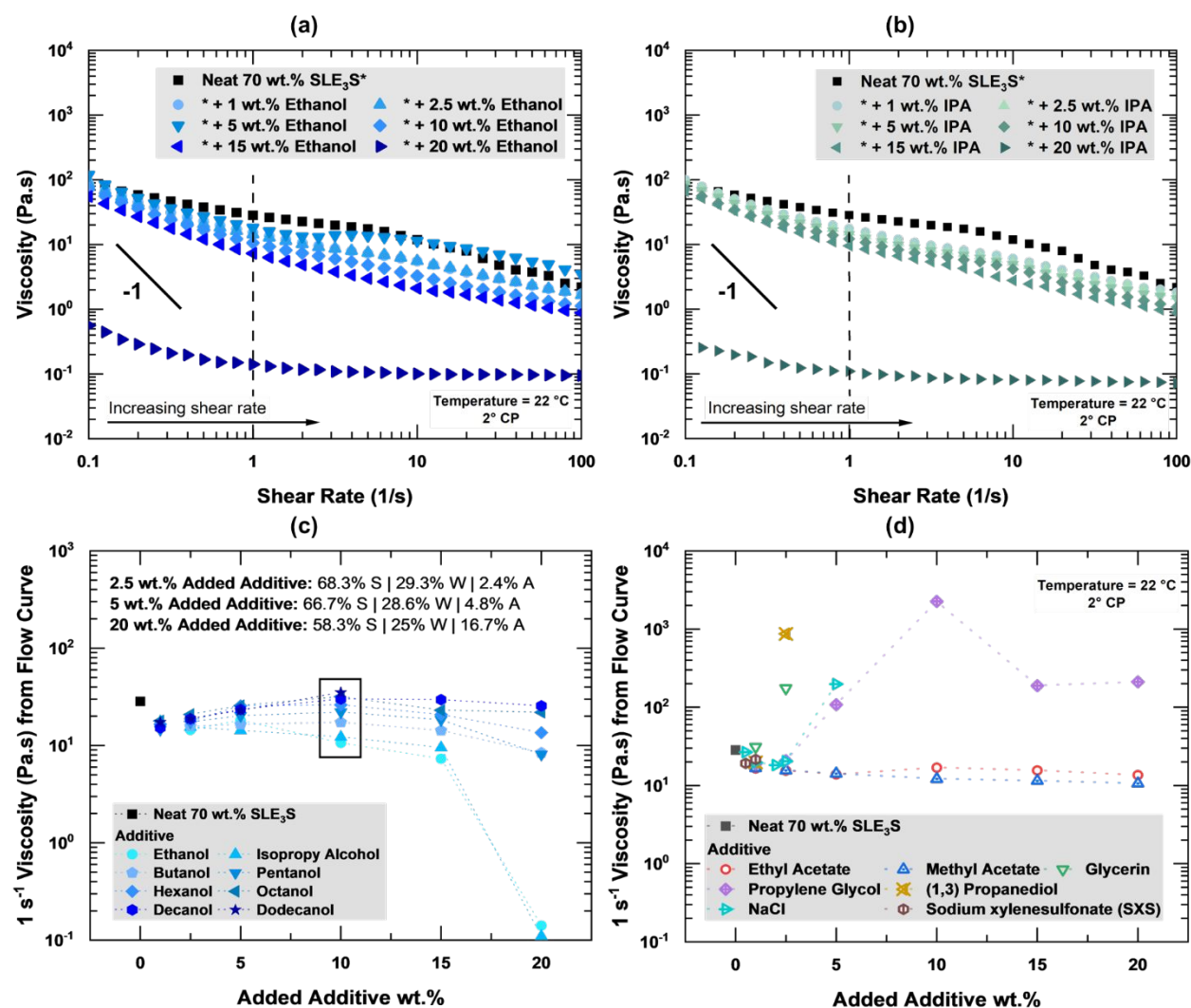


Figure 2. Effect of added (a) ethanol and (b) isopropyl alcohol (IPA) on the rheology of feedstock lamellar pastes, (c) 1 s^{-1} viscosity with increasing linear alcohol chain length and (d) 1 s^{-1} viscosity with increasing concentrations of acetates, polyols, hydrotrope (SXS) and salt. Solid black lines represent a slope of -1. Measured viscosities have an uncertainty of $\pm 5\%$ and all flow



curves are presented in **Supplementary Figures S6** and **Supplementary Figure S7**.

Concentration and additive dependent phases, 1 s^{-1} viscosity, Herschel-Bulkley fits for shear

stress vs. shear rate at low shear rates (**Supplementary Figure S8**) and d-spacings are all

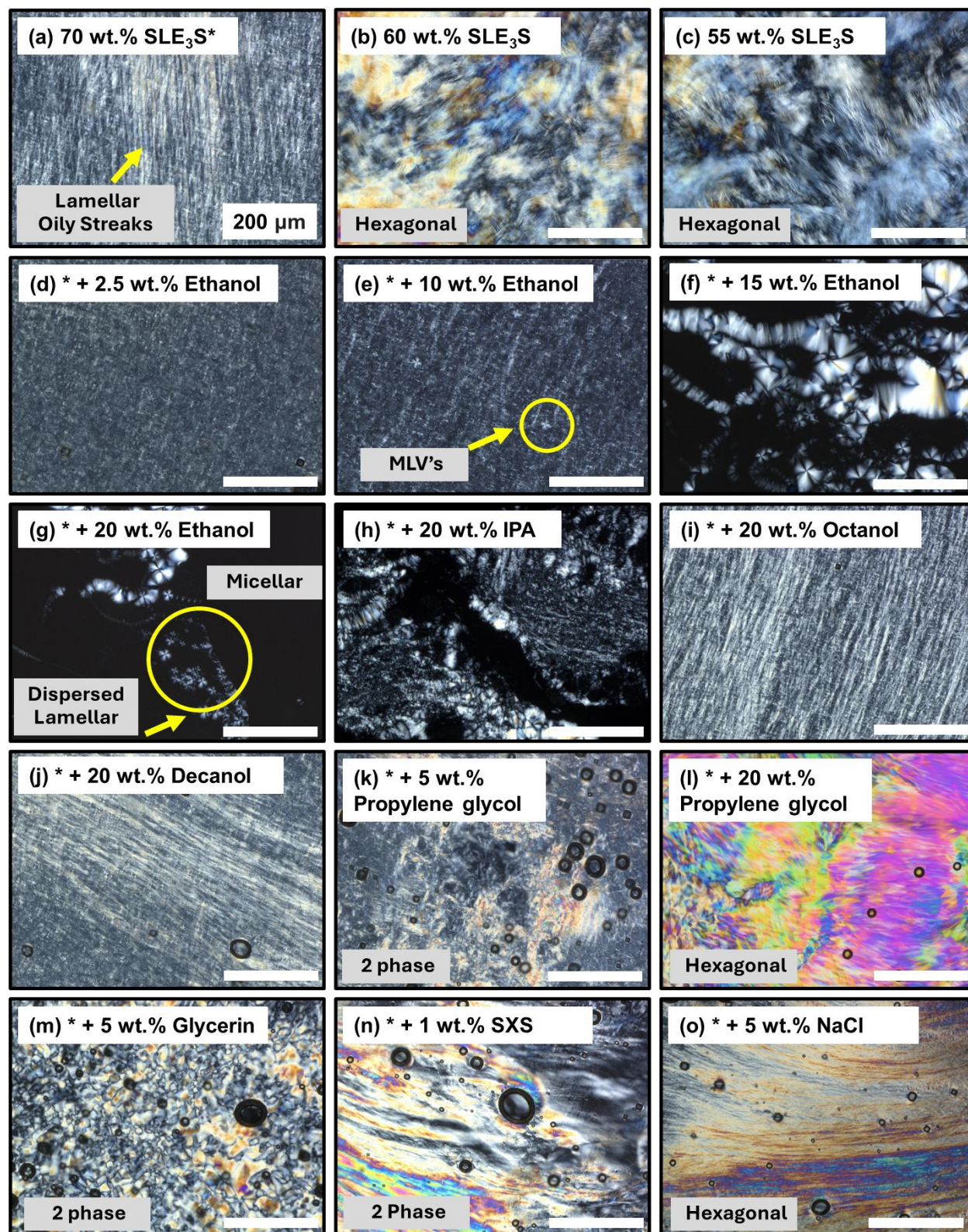
tabulated in **Supplementary Table T1**. Dynamic changes in microstructure under applied shear

for the sample with 15 wt.% ethanol are shown in **Supplementary Video V1**.

There is a substantial body of work studying alcohol-lipid bilayer interactions,^{93,94} and the effect of short-chain linear alcohols observed here was consistent with previous findings for some other dilute surfactant systems. Friberg *et al.*⁹⁵ reported the formation of a low viscosity liquid with the addition of ethanol to the didodecyldimethylammonium bromide (DDAB)-water lamellar phase. Dynamic light scattering was used to identify the presence of aggregates in the isotropic phase. Chen *et al.*⁹⁶ and Han *et al.*⁹⁷ developed injectable low viscosity solutions by using ethanol to induce liquid-crystalline-isotropic phase transitions in the phytantriol-water system. Alam used differing wave spectroscopy (DWS) and micro-rheology measurements to investigate the effect of ethanol concentration and temperature on phase transitions in the Dimodan U/J monoglyceride-water system.⁹⁸ In contrast, longer-chain alcohols (C_6 - C_{12}) and acetates exhibit lower solubility and preferentially partition near hydrophobic surfactant tails, acting like co-surfactants (Figure 2(c) and Figure 2(d)).⁹⁹ At the highest added dodecanol concentration (20 wt.%), two lamellar phases coexisted with d-spacings of $46.5 \pm 0.5 \text{ \AA}$ and $55.3 \pm 0.8 \text{ \AA}$. The lamellar phase with the higher d-spacing was more ordered (**Supplementary Figure S9**). The polyols, sodium xylenesulfonate and salt promoted formation of high viscosity hexagonal and mixed phases (Figure 2(d) and Figure 3 (k)-(o)).



407



408



Figure 3. (a) Neat 70 wt.% lamellar SLE₃S with oily streaks and multilamellar vesicles (MLV's), (b) and (c) hexagonal 60 wt.% and 55 wt.% water-diluted SLE₃S control microstructures respectively. The effective surfactant concentrations for several systems with additives fall in this range. Evolution of lamellar microstructure (a) with added linear chain alcohols: (d) - (g) ethanol, (h) isopropyl alcohol (IPA), (i) octanol and (j) decanol, (k) - (o) hexagonal and mixed phases at low added propylene glycol, glycerin, sodium xylenesulfonate (SXS) and salt concentrations. Qualitative identification of phase structures is based on work by Rosevear.¹⁰

Approach 2: Heating to approach upper temperature limit of liquid crystalline phases. Temperature-dependent viscosity reductions, azeotropic reactions¹¹ and other thermotropic transitions have been widely studied.^{100,101} In some systems such as aqueous non-ionic pentaethylene glycol monodecyl ether (C₁₀E₅), modest temperatures (~35 °C) are sufficient to induce liquid crystalline-to-micellar transitions,¹⁰² while in the linear alkylbenzene sulfonate-water system studied by Stewart *et al.*, changes in headgroup-counterion interactions at elevated temperatures played a significant role.¹⁰³ Figure 4 shows the temperature-dependent complex viscosity of 70 wt.% SLE₃S paste with added polyols. While rheometry experiments were conducted within the linear viscoelastic regime, static SAXS (Figure 5) was used to confirm that observed transitions were not shear-induced and reflected equilibrium behavior. Neat 70 wt.% SLE₃S had a nearly constant complex viscosity (~108 Pa s) and lamellar structure (Figure 5(a)) upon heating from 20 °C up to 90 °C, consistent with prior observations by Kelkar *et al.*²⁸ and Ferraro *et al.*^{33,34} Ongoing work is exploring the interesting shift in the scattering peak (q^*) toward lower Bragg spacings with increasing temperature.



At 20 °C, the 20 wt.% propylene glycol (PG) sample was hexagonal with a characteristic spacing of 49.2 ± 0.4 Å (Figures 3(l) and Figure 5(c)) and a complex viscosity of ~ 1130 Pa·s. Upon heating, the hexagonal phase persisted up to ~ 70 °C, beyond which higher-order SAXS peaks disappeared, and the complex viscosity dropped sharply to ~ 0.2 Pa s at 80 °C, indicating a transition to an isotropic phase with a micellar separation length of 40.6 ± 2.9 Å. In contrast, the 5 wt.% glycerin sample was biphasic with at least one lamellar phase at 20 °C (d-spacing equal to 46.1 ± 0.5 Å and 56.7 ± 0.3 Å; Figure 3(m) and Figure 5(b)) with very high complex viscosity (~ 9248 Pa·s). While it did not transition into a micellar solution, the complex viscosity of the lamellar phase (d-spacing of 44 ± 0.4 Å) at 50 °C (~ 25 Pa s) was significantly lower than neat SLE₃S.

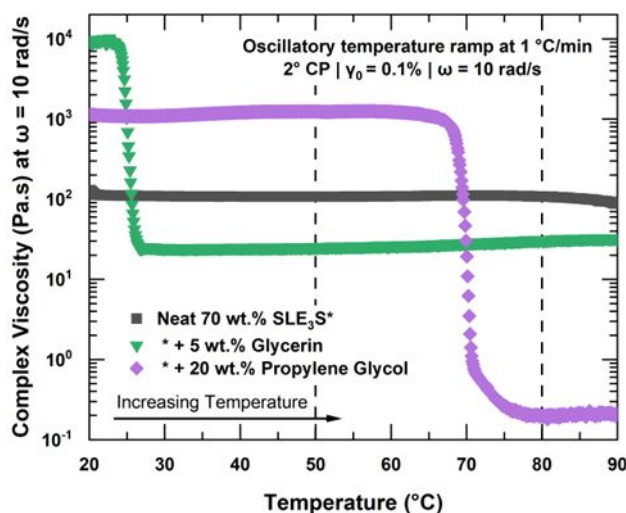


Figure 4. Evolution of complex viscosity measured during a continuous oscillatory temperature ramp from 20 °C to 90 °C. Hexagonal to micellar phase transition for specimen with 20 wt.% propylene glycol is reversible and significant hysteresis was not observed during the heating and cooling process (Supplementary Figure S10). It is key to note that temperature-driven phase transitions have both thermodynamic and kinetic aspects. Because equilibrium is



governed by both heat and mass transport, the temperature ramp rate can influence observed changes.¹¹

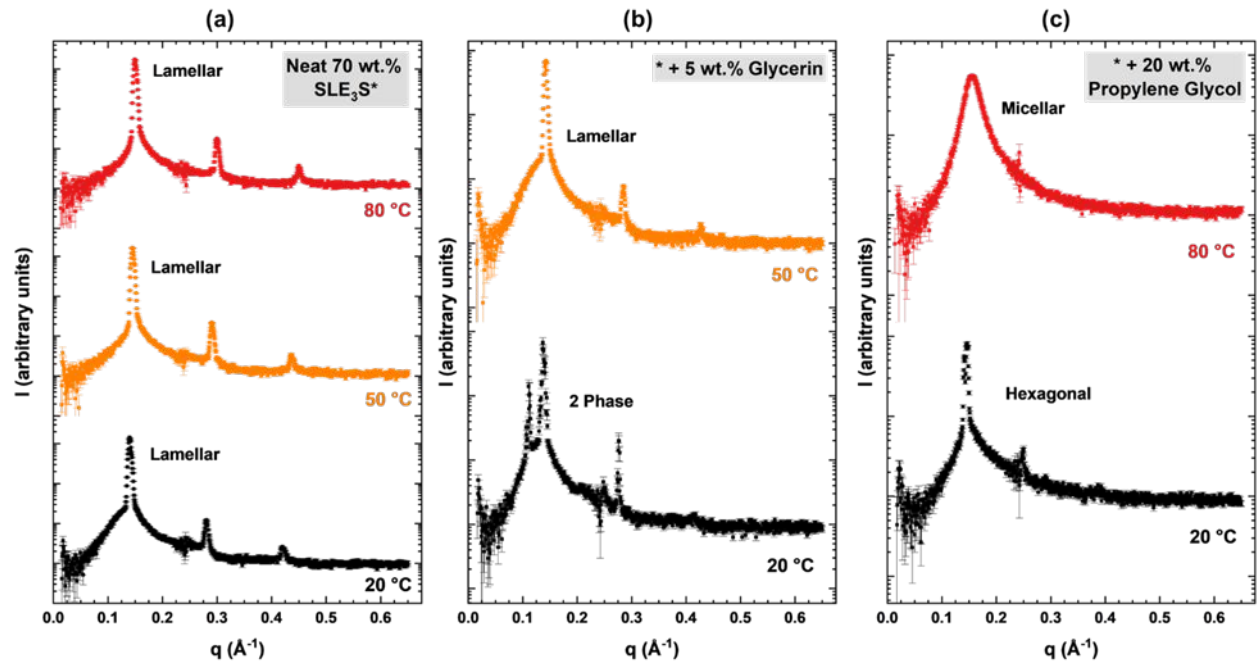


Figure 5. Effect of heating on SAXS patterns of (a) neat 70 wt.% SLE₃S, (b) +5 wt.% glycerin, and (c) +20 wt.% propylene glycol. Lamellar phases have characteristic peaks at q^* , $2q^*$ and $3q^*$ while hexagonal phases have peaks at q^* , $\sqrt{3}q^*$ and $2q^*$.⁵⁶ Room temperature cross-polarized micrographs are presented in Figure 3(a), (l) and (m), and 2D scattering patterns are presented in **Supplementary Figure S11**.

Polyols are water-soluble plasticizers and it is hypothesized that multiple hydroxyl groups (**Supplementary Figure S1**) enable strong interactions with anionic SLE₃S headgroups through hydrogen bonding.¹⁰⁴ These disrupt headgroup-water hydrogen bonds, potentially forming headgroup-polyol and water-polyol hydrogen bonds.¹⁰⁵ Thus, glycerin, with three hydroxyl groups, can form more hydrogen bonds than PG, which has two.¹⁰⁶ This is consistent with 1 s^{-1} viscosity measurements at 1 wt.% added additive (Figure 1(d) and **Supplementary Figure S7**),

where the glycerin-containing sample had a higher viscosity (~ 31 Pa·s) than the sample with PG (~ 18 Pa·s). In the concentration range studied here, both glycerin and propylene glycol increase effective headgroup area, shift the CPP, and promote curvature,¹⁰⁷ leading to the formation of hexagonal phases. As temperature rises, thermal motion and molecular disorder increase and liquid crystals transition to an isotropic solution.^{108,109} Hence, when PG-induced hexagonal phases are heated, hydrogen bonding weakens^{110,111} reducing effective headgroup area. This changes the CPP again resulting in a hexagonal-to-micellar transition.

Approach 3: Processing within the lamellar phase. The effects of propylene glycol (PG) and sodium chloride (NaCl) on the lamellar phase boundaries, rheology and microstructure evolution were studied in detail. Flow-phase diagrams developed by overlaying static phase information on viscosity values extracted from flow curves are presented in Figure 6, while Figure 7 and Figure 8 show the evolution of lamellar microstructure with added PG and NaCl respectively. High viscosities for the neat 70 wt.% SLE₁S solution at 5 °C and 10 °C are attributed to the presence of crystalline domains.²⁸ Behavior above room temperature is consistent with earlier observations here and in studies by Ferraro *et al.*^{33,34} and Kelkar *et al.*²⁸ In single-phase regions at fixed additive concentration, the viscosity at 1 s^{-1} , yield stress, and flow stress (**Supplementary Figure S12 and S13**) all decreased with increasing temperature. The yield stress is defined as the applied stress at which irreversible plastic deformation is first observed across the sample, typically obtained by fitting a Herschel-Bulkley model and extrapolating to zero shear rate. The flow stress is the value of the shear stress at the crossover point in an amplitude sweep.^{12,112} In all cases, the flow stress was numerically higher than the yield stress, potentially making it a more conservative parameter for predicting product stability and designing startup protocols in pumping to avoid stress overshoots and mechanical damage.¹¹³ At 20 °C, 5 wt.% propylene glycol had a



yield stress of ~4 Pa and a flow stress of ~23 Pa while for 1 wt.% NaCl, the corresponding values were ~23 Pa and ~65 Pa. Trends in two-phase regions were more complex, varying with relative proportions of coexisting phases.

At room temperature (~20 °C), increasing PG concentration within the lamellar region had minimal effect on 1 s⁻¹ viscosity, yield stress, and flow stress up to 5 wt.%, with more pronounced reductions observed only at 10 wt.% PG, where the lowest 1 s⁻¹ viscosity (~9.5 Pa·s) was measured. Compared to SLE₃S, the SLE₁S system exhibited a broader lamellar phase window with PG addition: while SLE₃S transitioned to a biphasic (lamellar and hexagonal) phase at PG concentrations as low as 5 wt.%, SLE₁S retained a lamellar phase up to at least 10 wt.%. The wider lamellar phase band in SLE₁S is likely due to its lower average degree of ethoxylation and associated PG-headgroup interactions.³³ Within the lamellar phase, for both systems, the 1 s⁻¹ viscosities were comparable: SLE₁S + 2 wt.% PG had viscosity of ~14 Pa s, while SLE₃S + 1 wt.% PG had a viscosity of ~19 Pa s.

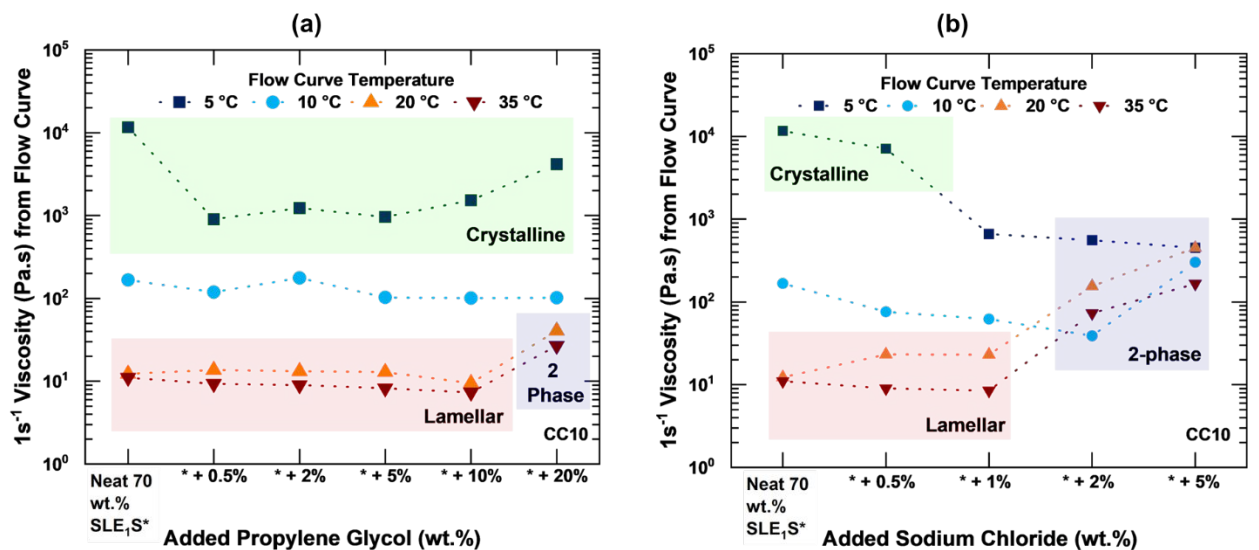


Figure 6. Flow-phase diagrams for added (a) propylene glycol and (b) NaCl. Static phase information determined from cross-polarized optical microscopy and SAXS. Full flow curves, corresponding Herschel-Bulkley fits at low shear rates and flow stresses from amplitude sweeps are presented in **Supplementary Figure S12** and **Supplementary Figure S13** respectively.

In contrast, salt produced a different response. Increasing the salt concentration led to a steady rise in 1 s^{-1} viscosity, yield stress, and flow stress within the lamellar phase. Across bulk SLE□S systems the response was almost invariant with changing degree of ethoxylation. The lamellar phase boundaries between SLE₁S and SLE₃S (> 2 wt.%), and the 1 s^{-1} viscosities at 1 wt.% NaCl (~23 Pa s for SLE₁S, ~20 Pa s for SLE₃S), were comparable. Salt affects charge screening around charged surfactant headgroups, potentially reducing headgroup repulsion and inducing phase transitions. This behavior has been studied extensively.^{15,114–117}

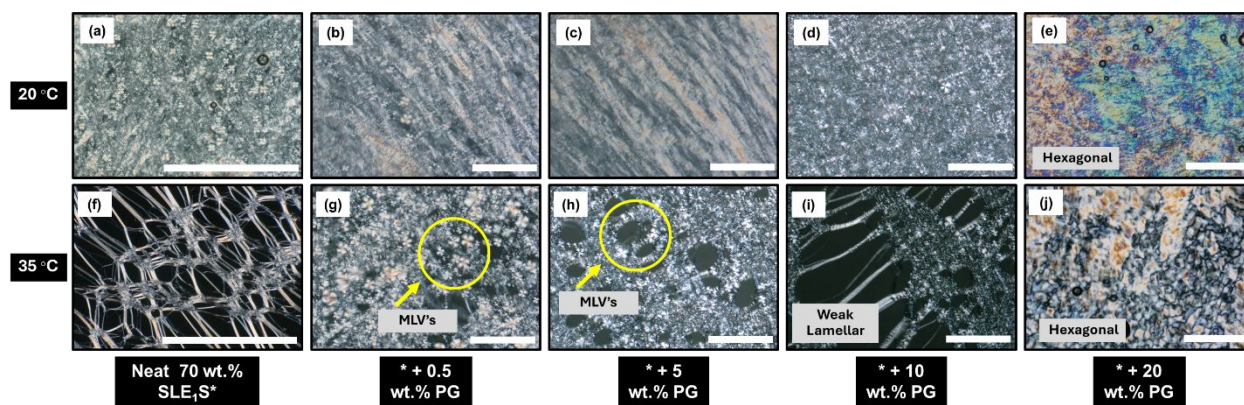


Figure 7. Evolution of static microstructure with added propylene glycol at 20 °C and 35 °C. Neat Lamellar SLE₁S micrographs reproduced from Kelkar *et al.*²⁸ Big scale bars in (a) and (f) represent 1 mm while smaller bars represent 100 μm.

Similar trends were observed in the static microstructure at 25 °C and 35 °C. With PG, increasing concentration and temperature progressively weakened the lamellar texture and



promoted the formation of multilamellar vesicles (MLVs) (Figure 7 (g) and Figure 7 (h)). In contrast, while higher temperatures led to more MLVs with NaCl (Figure 8 (g)), increasing salt concentration at a fixed temperature produced fewer MLVs (Figure 8 (g) and Figure 8 (h)). Under applied shear, lamellar phases showed strong orientation of oily streaks, consistent with classical shear-induced alignment.^{15,24,25} Aligned bilayers can roll up to form MLVs,²⁶ a process generally described by a balance between curvature energy and compression energy.¹¹⁸ Studies investigating time-dependent evolution of microstructure and formation mechanisms of MLVs under shear, as a function of confinement, additives and temperature are ongoing.

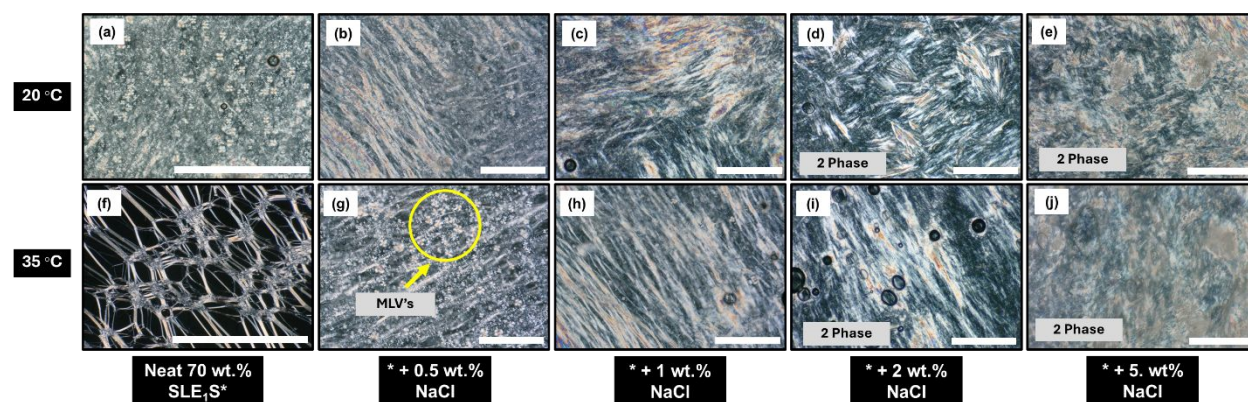


Figure 8. Evolution of static microstructure with added propylene glycol at 20 °C and 35 °C. Neat Lamellar SLE₁S micrographs reproduced from Kelkar *et al.*²⁸ Big scale bars in (a) and (f) represent 1 mm while smaller bars represent 100 μm.



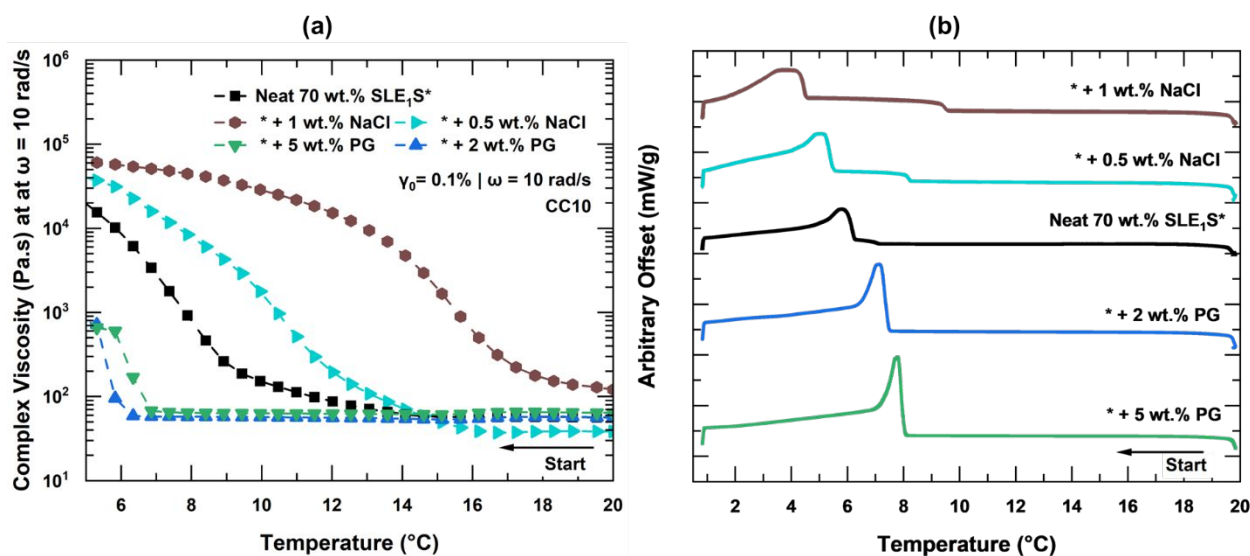


Figure 9. (a) Effect of small applied oscillations on the complex viscosity, and (b) equilibrium crystallization temperature range in a DSC ramp. Specimens were cooled from 20 $^{\circ}\text{C}$ to 5 $^{\circ}\text{C}$ at 1 $^{\circ}\text{C}/\text{min}$. Onset of crystallization is inferred from the drastic increase in complex viscosity during cooling.

The effect of small applied oscillations within the LVER on crystallization above the equilibrium crystallization temperature in neat lamellar phases has been previously studied by Kelkar *et al.*²⁸ At room temperature, the bulk lamellar phase has no crystals. As the solutions are slowly cooled, small oscillations primarily enhance growth. Inspired by the classical work of Nyvlt *et al.*¹¹⁹ on the theory of metastable zones, samples with added PG and NaCl were cooled and the results are presented in Figure 9.

Samples with added salt promoted crystallization at significantly higher temperatures than both neat 70 wt.% SLE₁S and solutions with added PG. The onset temperature was also much higher than the equilibrium crystallization temperature measured by DSC and increased with



544 increasing salt concentration. In contrast, as a known antifreeze agent,¹²⁰ PG extended the lamellar
545 phase region and suppressed crystallization. The onset of shear-induced crystallization was
546 restricted to temperatures close to the equilibrium DSC range. Increasing PG concentration from
547 2 wt.% to 5 wt.% had little additional effect, as both samples had nearly identical complex viscosity
548 trends during cooling.

549 Macroscopic rheological measurements through flow curves provide valuable insight into
550 bulk behavior, but internal velocity fields under shear can diverge significantly due to evolution
551 of flow instabilities like wall slip and plug flow.¹²¹ Wall slip refers to relative motion between the
552 material and the boundary, resulting in a discontinuity at the wall that manifests as a sliding of the
553 material along the surface. As the rheometer assumes a no-slip condition, wall slip leads to an
554 apparent reduction in viscosity.¹²² Plug flow describes uniform bulk translation with constant
555 velocity across the gap where flow arises from wall slip occurring simultaneously at both confining
556 surfaces.¹²³ A detailed investigation of non-homogeneous flow phenomena across different SLE₁S
557 phases was undertaken by Caicedo-Casso *et al.*¹⁵ their results showed that while lamellar phases
558 typically exhibit plug flow at low and intermediate shear rates, the neat 70 wt.% SLE₁S sample
559 approached a simple shear velocity profile at 70 s⁻¹, though some slip near the rotor remained
560 evident in the velocity profiles.

561 Velocity profiles for neat 70 wt.% aqueous solutions of SLE₁S, SLE₂S, and SLE₃S at shear
562 rates of 7 s⁻¹ and 70 s⁻¹ are presented in **Supplementary Figure S14**. Across all feedstock
563 solutions, velocity profiles were qualitatively similar. At 7 s⁻¹, plug-like flow was observed, with
564 near-uniform velocity in the gap and minor gradients near the boundaries. At 70 s⁻¹, each system
565 exhibited simple shear near the stator and slip near the rotor, suggesting stress localization across
566 the gap and the possible onset of shear banding. Lamellar-structured SLE₁S matched the profile



reported by Caicedo-Casso *et al.*¹⁵ only in isolated cases; more commonly, it slipped more near the rotor. These differences were not unexpected and are likely due to batch-to-batch variability.

The effects of PG addition are presented in Figure 10. At 7 s^{-1} , all samples showed plug-flow with nearly constant velocity across the gap (Figure 10(c)). The 10 wt.% PG sample slips more at both walls with the lowest velocity across the gap. It also shows the lowest measured shear stress on the flow curve - 28 Pa compared to 33 Pa for neat SLE₁S. The flow behavior was different at 70 s^{-1} - all specimens showed simple shear behavior closest to the stator and wall slip at the rotor. The 5 wt.% PG sample was like the neat SLE₁S, but the 10 wt.% PG solution slipped more (Figure 10(d)) and had the lowest measured shear stress ($\sim 107 \text{ Pa}$ vs. $\sim 116 \text{ Pa}$ for neat SLE₁S; Figure 10(b)). However, the normalized velocity near the rotor was slightly higher than that observed at 7 s^{-1} . This is likely due to wall slip being more dominant at lower shear rates.^{112,124}



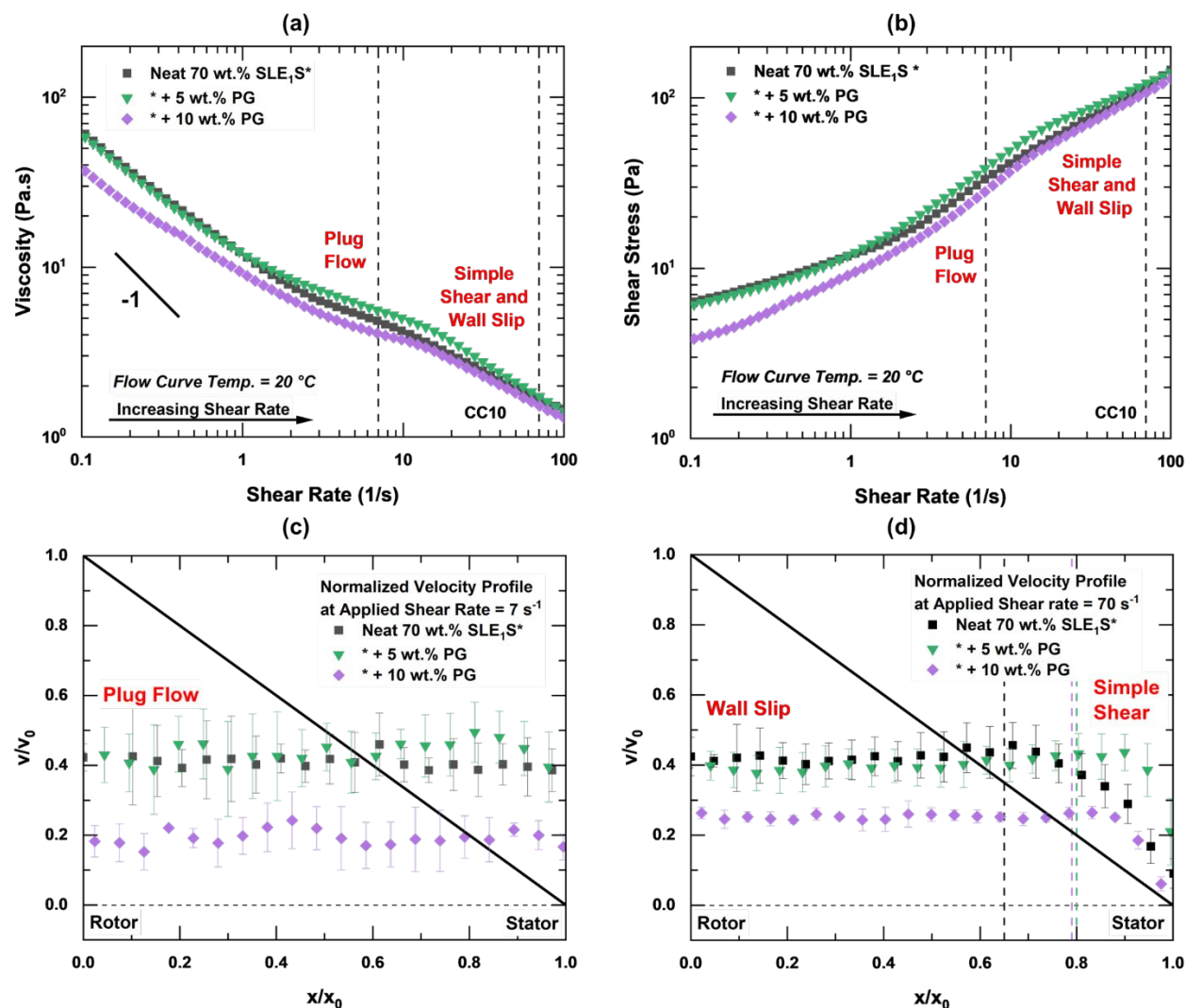


Figure 10. Effect of propylene glycol (PG) addition on bulk rheology and velocity profiles of 70 wt.% SLE₁S solutions. (a) and (b) viscosity and shear stress as a function of shear rate at 20 °C. Vertical dashed lines indicate shear rates corresponding to USV measurements, (c) and (d) normalized velocity profiles at 7 s⁻¹ and 70 s⁻¹. Solid black line indicates slope of -1.

The increase in slip with 10 wt.% PG addition, suggests that PG alters bilayer-shearing surface interactions. As a plasticizer, it weakens the lamellar structure (Figure 7 (c), (e) and (g)) and the less structured lamellar bilayers may align more readily under shear, acting as localized



lubrication layers. Since increased surface roughness reduces wall slip,¹²⁵ formation of aligned PG-rich bilayers should have the opposite effect and facilitate slip. These observations are consistent with a slip-film mechanism,¹²⁶ where a structurally relaxed or weaker layer near the rotor wall accommodates shear independently of the bulk. Due to instrumental resolution limitations, the thickness of such a layer is not directly measured here, but the combination of increased slip and weakened structure supports this interpretation. For more detailed discussions of flow instabilities in complex fluids, the reader is directed to the works of Divoux *et al.*,¹²⁴ Cloitre and Bonnecaze,¹²⁷ and Malkin and Patlazhan.¹²⁸



IMPLICATIONS

Processing highly viscous, concentrated feedstocks is a key challenge in surfactant manufacturing. Upstream operations routinely face a cost-driven trade-off between increased energy demands for processing and the added complexity of introducing additives. The primary goal of utilizing additives is to maintain high activity while reducing viscosity, and the strategies demonstrated here (summarized in Figure 11) with lamellar phases suggest that this constraint may not be absolute.

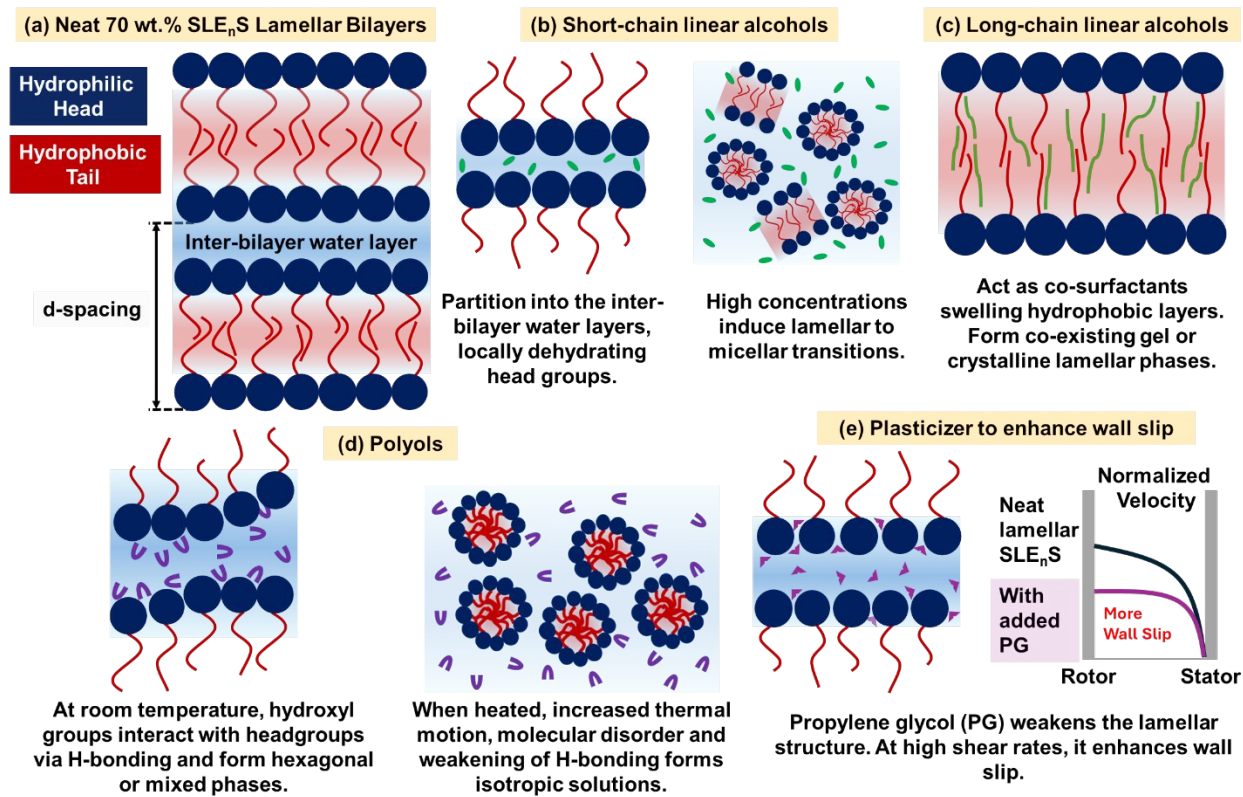


Figure 11. Schematic of three approaches to simplify processing of concentrated feedstock pastes. (a) structure of the lamellar feedstock, (b) and (c) Approach 1: linear chain alcohols, (d) Approach 2: Heating to approach upper temperature limit of liquid crystalline phases, and (e) Approach 3: processing within the lamellar phase by enhancing wall slip.

Adapted and modified from Seddon and Templer,¹²⁹ Kulkarni,¹³⁰ Radaic *et al.*,¹³¹ and Steck *et al.*¹³²

Short-chain alcohols effectively reduced viscosity, but flammability and volatility concerns may limit their use in early-stage processing - particularly in heated premix vessels or open transfer systems. When introduced too early, alcohols can limit the use of temperature as a downstream processing lever, requiring all subsequent additives to be miscible at lower temperatures and not induce liquid-crystalline order. While counterintuitive, passing through a hexagonal phase before heating, despite its higher viscosity, can lead to lower viscosity manufacturing pathways. In typical manufacturing processes, a formula may be structured into a hexagonal phase and held hot in a jacketed main mix tank to induce a transition to a micellar solution. After this, performance ingredients like conditioning polymers or mildness boosters can be introduced while the system is still hot followed by alcohols during cooling to tune rheology. A similar order-of-addition dependence has been reported for feedstock alkyl ether sulfate systems, where ionic liquid-alcohol blends reduced viscosity only when introduced together at low concentrations; when added separately, they had little to no effect.¹³³

Hexagonal phases formed inside pipe loops – often triggered by trace water and thought to be irreversible, can catastrophically obstruct handling and compromise throughput. In some cases, entire sections must be replaced, resulting in costly downtime. But, if they are intentionally formed with the right additives in tanks or vessels that can be heated and mixed, they are more manageable and even useful. At room temperature, their high viscosity and yield stress can help prevent spills or dripping. In solutions that remain lamellar throughout processing, flow can be tuned without inducing bulk phase transitions. Additives that induce wall slip and suppress shear-induced



642 crystallization can improve flow rates^{134,135} and reduce the formation of high-viscosity crystalline
643 phases in pipes and pumps under minor temperature variations.

644 Beyond lamellar SLE_nS systems, formulators should first identify the liquid crystalline
645 phase formed by their concentrated feedstock without additives using a simple dilution series and
646 cross-polarized optical microscopy. The combination of approaches needed to reach a low-
647 viscosity micellar solution will depend on this initial phase, since efficient trajectories through
648 complex phase diagrams necessitate a clearly defined starting point. Instead of relying on
649 simplistic CPP or hydrophilic-lipophilic balance (HLB), the hydrophilic-lipophilic deviation
650 (HLD)-net average curvature (NAC) framework offers a quantitative basis for anticipating how
651 additives can modify spontaneous curvature.^{136,137} In systems containing oils, fragrances, or co-
652 solvents, shifts in effective alkane carbon number (EACN) become equally important.¹³⁷ The
653 additive effects demonstrated here can be reinterpreted through this lens. When designed to
654 selectively target the headgroup, tail, or water layers, additive blends can tune rheology, suppress
655 shear-induced crystallization and function as value-added formulation ingredients.

656

657

658

659

660

661

662



CONCLUSIONS

In this experimental study, three additive-driven approaches to tune the rheology and microstructure of concentrated lamellar structured 70 wt.% SLE_nS-water systems are demonstrated (Figure 11). Short-chain alcohols such as ethanol and isopropyl alcohol reduced viscosity by locally dehydrating headgroups and inducing lamellar-to-micellar transitions at high concentrations (Figure 2 and Figure 3 (d) – (h)). Glycerin and propylene glycol interact with SLE_nS headgroups via hydrogen bonding, inducing lamellar-to-hexagonal or mixed-phase transitions at room temperature, and form micellar liquids upon heating beyond the upper temperature limit of liquid crystalline phases (Figure 4 and Figure 5).

Within the lamellar phase, PG weakened bilayer structure (Figure 7), suppressed shear-induced crystallization (Figure 9) and enhanced wall slip at high shear rates (Figure 10). Its effects also depended more strongly on the degree of ethoxylation than those of salt. By contrast, NaCl led to higher-viscosity biphasic regions at low concentrations (Figure 6 and Figure 8) and promoted shear-induced crystallization above the equilibrium crystallization temperature (Figure 9). Datasets developed here - linking additive structure to rheology, d-spacing, and yield stress - can further support modeling efforts aimed at designing tailor-made molecules to achieve targeted flow and structural outcomes. Workflows developed here for SLE_nS systems provide a foundation for optimizing processing and enabling the sustainable design and manufacturing of concentrated surfactant-based products.



AUTHOR CONTRIBUTIONS

P.U.K.: conceptualization, data curation, formal analysis, investigation, methodology, visualization, writing - original draft; M.K.: data curation, formal analysis, investigation, methodology, visualization, writing - review & editing; C.A.A.: investigation, writing – review & editing; E.R.W.: investigation, writing - review & editing; S.L.: conceptualization, funding acquisition, resources, writing - review & editing; K.A.E.: conceptualization, data curation, funding acquisition, project administration, visualization, supervision, writing - original draft, writing - review & editing.

ELECTRONIC SUPPLEMENTARY INFORMATION

Molecular structures of all molecules, characterization of various SLE_nS feedstocks, calibration curves for the rheo-USV, SAXS patterns for key phases and transitions, full flow curves and shear stress vs shear rate data at low shear rates with tabulated Herschel-Bulkley fits for all additives, amplitude sweeps and flow stress at different temperatures, rheo-USV velocity profiles of neat SLE_nS feedstocks.

CONFLICTS OF INTEREST

There are no conflicts of interest to declare.

DATA AVAILABILITY

Data supporting this article have been included as part of the supplementary information.

ACKNOWLEDGEMENTS

P.U.K. and K.A.E. acknowledge support from the National Science Foundation (NSF) through GOALI Grant No. CBET-2112956.

706



707 REFERENCES

- 708 1 J. Scamehorn, D. Sabatini and J. Harwell, in *Encyclopedia of Supramolecular Chemistry*,
709 CRC Press, Boca Raton, 1st edn., 2004.
- 710 2 J. Scamehorn, D. Sabatini and J. Harwell, in *Encyclopedia of Supramolecular Chemistry*,
711 CRC Press, Boca Raton, 1st edn., 2004.
- 712 3 S. Liu, L. G. Papageorgiou and N. Shah, *Comput Ind Eng*, 2020, **139**, 106189.
- 713 4 J. Cosby, PhD thesis, University of Sheffield, 2021.
- 714 5 E. Saouter, G. van Hoof, C. A. Pittinger and T. C. J. Feijtel, *Int J Life Cycle Assess*, 2001,
715 **6**, 363–372.
- 716 6 M. Giagnorio, A. Amelio, H. Grüttner and A. Tiraferri, *J Clean Prod*, 2017, **154**, 593–
717 601.
- 718 7 F. Mattos Batista de Moraes, L. Kulay and A. Trianni, *Sustain Prod Consum*, 2025, **55**,
719 76–89.
- 720 8 I. E. M. O. de Moura and E. A. da Silva, *International Journal of Environmental Science*
721 *and Technology*, 2024, **21**, 3235–3256.
- 722 9 R. Zana, *Dynamics of Surfactant Self-Assemblies*, CRC Press, 1st edn., 2005.
- 723 10 F. B. Rosevear, *J Am Oil Chem Soc*, 1954, **31**, 628–639.
- 724 11 R. G. Laughlin, *The Aqueous Phase Behavior of Surfactants*, Academic Press, 1994.
- 725 12 R. G. Larson, *The Structure and Rheology of Complex Fluids*, Oxford Academic Press,
726 1998.
- 727 13 J. N. Israelachvili, D. J. Mitchell and B. W. Ninham, *Journal of the Chemical Society*,
728 *Faraday Transactions 2*, 1976, **72**, 1525.
- 729 14 P. A. Hassan, G. Verma and R. Ganguly, in *Functional Materials*, Elsevier, 2012, pp. 1–
730 59.
- 731 15 E. A. Caicedo-Casso, J. E. Bice, L. R. Nielsen, J. L. Sargent, S. Lindberg and K. A. Erk,
732 *Rheol Acta*, 2019, **58**, 467–482.
- 733 16 E. F. Marques and B. F. B. Silva, in *Encyclopedia of Colloid and Interface Science*,
734 Springer Berlin Heidelberg, Berlin, Heidelberg, 2013, pp. 1290–1333.
- 735 17 M. Aljabri and T. Rodgers, *ACS Physical Chemistry Au*, 2024, **4**, 490–498.
- 736 18 P. Kelkar, M. Caggioni, K. Erk and S. Lindberg, *Langmuir*,
737 DOI:https://doi.org/10.1021/acs.langmuir.4c05057.



- 738 19 A. Capaccio, S. Caserta, S. Guido, G. Rusciano and A. Sasso, *J Colloid Interface Sci*,
739 2020, **561**, 136–146.
- 740 20 R. H. Ewoldt, M. T. Johnston and L. M. Caretta, 2015, pp. 207–241.
- 741 21 D. Coles, *J Fluid Mech*, 1965, **21**, 385–425.
- 742 22 C. D. Andereck, S. S. Liu and H. L. Swinney, *J Fluid Mech*, 1986, **164**, 155–183.
- 743 23 M. Włodzimierz Sulek and A. Bak, *Int J Mol Sci*, 2010, **11**, 189–205.
- 744 24 P. Sierro and D. Roux, *Phys Rev Lett*, 1997, **78**, 1496–1499.
- 745 25 O. Diat, D. Roux and F. Nallet, *Journal de Physique II*, 1993, **3**, 1427–1452.
- 746 26 D. Roux, F. Nallet and O. Diat, *Europhysics Letters (EPL)*, 1993, **24**, 53–58.
- 747 27 M. G. Berni, C. J. Lawrence and D. Machin, *Adv Colloid Interface Sci*, 2002, **98**, 217–
748 243.
- 749 28 P. U. Kelkar, M. Kaboolian, R. D. Corder, M. Caggioni, S. Lindberg and K. A. Erk, *Soft*
750 *Matter*, 2024, **20**, 3299–3312.
- 751 29 P. Kékicheff, C. Grabielle-Madelmont and M. Ollivon, *J Colloid Interface Sci*, 1989, **131**,
752 112–132.
- 753 30 R. I. Castaldo, R. Pasquino, M. M. Villone, S. Caserta, C. Gu, N. Grizzuti, S. Guido, P. L.
754 Maffettone and V. Guida, *Soft Matter*, 2019, **15**, 8352–8360.
- 755 31 R. L. Hendrikse, A. E. Bayly and P. K. Jimack, *J Phys Chem B*, 2022, **126**, 8058–8071.
- 756 32 R. L. Hendrikse, A. E. Bayly, P. K. Jimack and X. Lai, *J Phys Chem B*, 2023, **127**, 4676–
757 4686.
- 758 33 R. Ferraro, M. Michela Salvatore, R. Esposito, S. Murgia, S. Caserta, G. D’Errico and S.
759 Guido, *J Mol Liq*, 2024, **405**, 124990.
- 760 34 R. Ferraro and S. Caserta, *Rheol Acta*, 2023, **62**, 365–375.
- 761 35 S. Abbott, Pure versus Commercial Surfactants, [https://www.stevenabbott.co.uk/practical-](https://www.stevenabbott.co.uk/practical-surfactants/Pure-Commercial.php)
762 [surfactants/Pure-Commercial.php](https://www.stevenabbott.co.uk/practical-surfactants/Pure-Commercial.php), (accessed 19 May 2025).
- 763 36 P. Romanowski and R. Schueller, *Beginning cosmetic chemistry : practical knowledge for*
764 *the cosmetic industry*, Allured Books, Carol Stream, 3rd edn., 2009.
- 765 37 M. Chandler and S. Gahan, Introducing the ‘4-P+ Process’ to Power Production of Natural
766 Products, [https://www.in-cosmetics.com/global/en-gb/show-programme/sessions-](https://www.in-cosmetics.com/global/en-gb/show-programme/sessions-details.4266.236496.Introducing%2Bthe%2B%25E2%2580%25984-P%252B%2BProcess%25E2%2580%2599%2Bto%2BPower%2BProduction%2Bof%2BNatural%2BProducts.html)
767 [details.4266.236496.Introducing%2Bthe%2B%25E2%2580%25984-](https://www.in-cosmetics.com/global/en-gb/show-programme/sessions-details.4266.236496.Introducing%2Bthe%2B%25E2%2580%25984-P%252B%2BProcess%25E2%2580%2599%2Bto%2BPower%2BProduction%2Bof%2BNatural%2BProducts.html)
768 [P%252B%2BProcess%25E2%2580%2599%2Bto%2BPower%2BProduction%2Bof%2B](https://www.in-cosmetics.com/global/en-gb/show-programme/sessions-details.4266.236496.Introducing%2Bthe%2B%25E2%2580%25984-P%252B%2BProcess%25E2%2580%2599%2Bto%2BPower%2BProduction%2Bof%2BNatural%2BProducts.html)
769 [Natural%2BProducts.html](https://www.in-cosmetics.com/global/en-gb/show-programme/sessions-details.4266.236496.Introducing%2Bthe%2B%25E2%2580%25984-P%252B%2BProcess%25E2%2580%2599%2Bto%2BPower%2BProduction%2Bof%2BNatural%2BProducts.html), (accessed 19 May 2025).
- 770 38 S. Abbott, in *Surfactant Science: Principles & Practice*, 1.0.7., 2024, pp. 198–213.



- 771 39 J. W. McBain and W. J. Elford, *J. Chem. Soc.*, 1926, **129**, 421–438.
- 772 40 P. Ekwall, in *Advances in Liquid Crystals*, 1975, vol. 1, pp. 1–142.
- 773 41 P. Ekwall, L. Mandell and K. Fontell, *J Colloid Interface Sci*, 1969, **29**, 639–646.
- 774 42 R. De Lisi and S. Milioto, *Chem. Soc. Rev.*, 1994, **23**, 67–73.
- 775 43 R. G. Laughlin, *J Am Oil Chem Soc*, 1990, **67**, 705–710.
- 776 44 A. Khan, *Curr Opin Colloid Interface Sci*, 1996, **1**, 614–623.
- 777 45 K. Holmberg, B. Jönsson, B. Kronberg and B. Lindman, in *Surfactants and Polymers in*
778 *Aqueous Solution*, Wiley, 2002, pp. 67–96.
- 779 46 H. Wennerström, *J Dispers Sci Technol*, 2007, **28**, 31–37.
- 780 47 I. M. Tucker, *Curr Opin Colloid Interface Sci*, 2024, **71**, 101789.
- 781 48 G. Rong and S. E. Friberg, *J Dispers Sci Technol*, 1988, **9**, 401–413.
- 782 49 S. E. Friberg and P. Liang, *Colloid Polym Sci*, 1986, **264**, 449–453.
- 783 50 M. Buzier and J.-C. Ravey, in *Surfactants in Solution*, Springer US, Boston, MA, 1986,
784 pp. 525–536.
- 785 51 R. Strey, *Berichte der Bunsengesellschaft für physikalische Chemie*, 1996, **100**, 182–189.
- 786 52 D. Roux, C. R. Safinya and F. Nallet, in *Micelles, Membranes, Microemulsions, and*
787 *Monolayers*, 1994, pp. 303–346.
- 788 53 A. S. Sadaghiani, A. Khan and B. Lindman, *J Colloid Interface Sci*, 1989, **132**, 352–362.
- 789 54 Y. Tokuoka, H. Uchiyama and M. Abe, *Colloid Polym Sci*, 1994, **272**, 317–323.
- 790 55 C. Ligoure, G. Bouglet and G. Porte, *Phys Rev Lett*, 1993, **71**, 3600–3603.
- 791 56 P. Alexandridis, U. Olsson and B. Lindman, *Langmuir*, 1998, **14**, 2627–2638.
- 792 57 Gunnar. Karlstroem, Anders. Carlsson and Bjoern. Lindman, *J Phys Chem*, 1990, **94**,
793 5005–5015.
- 794 58 M. Kahlweit, R. Strey, P. Firman and D. Haase, *Langmuir*, 1985, **1**, 281–288.
- 795 59 T. Wörnheim and A. Jönsson, *J Colloid Interface Sci*, 1988, **125**, 627–633.
- 796 60 T. Wörnheim, A. Jönsson and M. Sjöberg, in *Surfactants and Macromolecules: Self-*
797 *Assembly at Interfaces and in Bulk*, Steinkopff, Darmstadt, 1990, pp. 271–279.
- 798 61 K. P. Das, A. Ceglie, M. Monduzi, O. Söderman and B. Lindman, in *New Trends in*
799 *Colloid Science*, Steinkopff, Darmstadt, 1987, pp. 167–173.
- 800 62 N. Akter, S. Radiman, F. Mohamed, I. A. Rahman and M. I. H. Reza, *Sci Rep*, 2011, **1**, 71.



- 801 63 A. Baruah, A. K. Pathak and K. Ojha, *Ind Eng Chem Res*, 2015, **54**, 7640–7649.
- 802 64 Z. Zhong, G. Du, Y. Wang and J. Jiang, *Langmuir*, 2023, **39**, 11081–11089.
- 803 65 H. Honaryar, S. Amirfattahi, D. Nguyen, K. Kim, J. C. Shillcock and Z. Niroobakhsh,
804 *Small*, DOI:10.1002/sml.202403013.
- 805 66 K. A. Murthy and E. W. Kaler, *Colloid Polym Sci*, 1989, **267**, 330–335.
- 806 67 G. Montalvo, M. Valiente and E. Rodenas, *Langmuir*, 1996, **12**, 5202–5208.
- 807 68 A. Martino and E. W. Kaler, *Colloids Surf A Physicochem Eng Asp*, 1995, **99**, 91–99.
- 808 69 J. Yang, X. Wang, S. Ji, X. Wang, W. Qin and R. Li, *J Mol Liq*, 2016, **213**, 8–12.
- 809 70 R. A. Gonçalves, B. Lindman, M. G. Miguel, T. Iwata and Y. M. Lam, *J Colloid Interface*
810 *Sci*, 2018, **528**, 400–409.
- 811 71 R. A. Gonçalves, P. Naidjonoka, T. Nylander, M. G. Miguel, B. Lindman and Y. M. Lam,
812 *RSC Adv*, 2020, **10**, 18025–18034.
- 813 72 R. A. Gonçalves, Y.-M. Lam and B. Lindman, *Molecules*, 2021, **26**, 3946.
- 814 73 L. Piculell, *Langmuir*, 2013, **29**, 10313–10329.
- 815 74 A. Cukurkent and O. Masalci, *Colloid Polym Sci*, 2025, **303**, 301–312.
- 816 75 S. Khosharay, M. Rahmanzadeh and B. ZareNezhad, *Int J Thermophys*, 2020, **41**, 166.
- 817 76 F. Choi, R. Chen and E. J. Acosta, *J Colloid Interface Sci*, 2020, **564**, 216–229.
- 818 77 M. Pleines, W. Kunz, T. Zemb, D. Benczédi and W. Fieber, *J Colloid Interface Sci*, 2019,
819 **537**, 682–693.
- 820 78 A. Parker and W. Fieber, *Soft Matter*, 2013, **9**, 1203–1213.
- 821 79 M. Panoukidou, C. R. Wand, A. Del Regno, R. L. Anderson and P. Carbone, *J Colloid*
822 *Interface Sci*, 2019, **557**, 34–44.
- 823 80 M. T. Hossain and R. H. Ewoldt, *J Rheol (N Y N Y)*, 2024, **68**, 113–144.
- 824 81 J. E. Bice, Master of Science in Materials Science Engineering, Purdue University, 2017.
- 825 82 S. Manneville, L. Bécu and A. Colin, *The European Physical Journal Applied Physics*,
826 **2004**, **28**, 361–373.
- 827 83 J. S. Clunie, J. F. Goodman and P. C. Symons, *Transactions of the Faraday Society*, 1969,
828 **65**, 287.
- 829 84 J. W. Gibbs, *The Collected Works of J. Willard Gibbs*, Longmans, Green and Co., New
830 York, 1928, vol. Vol. I.
- 831 85 G. Kaptay, *Materials*, 2024, **17**, 6048.



- 832 86 Y. Yamashita, H. Kunieda, E. Oshimura and K. Sakamoto, *J Colloid Interface Sci*, 2007,
833 **312**, 172–178.
- 834 87 Y. Yamashita, in *Liquid Crystals - Recent Advancements in Fundamental and Device*
835 *Technologies*, InTech, 2018.
- 836 88 W. R. Klemm, *Alcohol*, 1990, **7**, 49–59.
- 837 89 S. Cinelli, G. Onori and A. Santucci, *Colloids Surf A Physicochem Eng Asp*, 1999, **160**, 3–
838 8.
- 839 90 L. Toppozini, C. L. Armstrong, M. A. Barrett, S. Zheng, L. Luo, H. Nanda, V. G. Sakai
840 and M. C. Rheinstädter, *Soft Matter*, 2012, **8**, 11839.
- 841 91 J.-S. Chiou, P. R. Krishna, H. Kamaya and I. Ueda, *Biochimica et Biophysica Acta (BBA)*
842 *- Biomembranes*, 1992, **1110**, 225–233.
- 843 92 F. Li, Z. Men, S. Li, S. Wang, Z. Li and C. Sun, *Spectrochim Acta A Mol Biomol*
844 *Spectrosc*, 2018, **189**, 621–624.
- 845 93 M. Patra, E. Salonen, E. Terama, I. Vattulainen, R. Faller, B. W. Lee, J. Holopainen and
846 M. Karttunen, *Biophys J*, 2006, **90**, 1121–1135.
- 847 94 H. A. Pillman and G. J. Blanchard, *J Phys Chem B*, 2010, **114**, 3840–3846.
- 848 95 S. E. Friberg, H. Hasinović, Q. Yin, Z. Zhang and R. Patel, *Colloids Surf A Physicochem*
849 *Eng Asp*, 1999, **156**, 145–156.
- 850 96 Y. Chen, X. Liang, P. Ma, Y. Tao, X. Wu, X. Wu, X. Chu and S. Gui, *AAPS*
851 *PharmSciTech*, 2015, **16**, 846–854.
- 852 97 K. Han, X. Pan, M. Chen, R. Wang, Y. Xu, M. Feng, G. Li, M. Huang and C. Wu,
853 *European Journal of Pharmaceutical Sciences*, 2010, **41**, 692–699.
- 854 98 M. M. Alam, *Liq Cryst*, 2012, **39**, 1427–1434.
- 855 99 S. Abbott, *Surfactant Science: Principles and Practice*, 2019, vol. 1.0.6.
- 856 100 H. Kunieda and F. Harigai, *J Colloid Interface Sci*, 1990, **134**, 585–588.
- 857 101 H. Kunieda and K. Nakamura, *J Phys Chem*, 1991, **95**, 1425–1430.
- 858 102 Y. Nibu and T. Inoue, *J Colloid Interface Sci*, 1998, **205**, 305–315.
- 859 103 J. A. Stewart, A. Saiani, A. Bayly and G. J. T. Tiddy, *Colloids Surf A Physicochem Eng*
860 *Asp*, 2009, **338**, 155–161.
- 861 104 Q. Li, X. Wang, X. Yue and X. Chen, *Langmuir*, 2015, **31**, 13511–13518.
- 862 105 N. H. Rhys, R. J. Gillams, L. E. Collins, S. K. Callear, M. J. Lawrence and S. E. McLain,
863 *J Chem Phys*, DOI:10.1063/1.4971208.



- 864 106 X. Pei, Y. You, J. Zhao, Y. Deng, E. Li and Z. Li, *J Colloid Interface Sci*, 2010, **351**, 457–
865 465.
- 866 107 K. Alfons and S. Engstrom, *J Pharm Sci*, 1998, **87**, 1527–1530.
- 867 108 A. de Vries, in *Liquid Crystals and Ordered Fluids*, Springer US, Boston, MA, 1984, pp.
868 137–153.
- 869 109 K. Aramaki, U. Olsson, Y. Yamaguchi and H. Kunieda, *Langmuir*, 1999, **15**, 6226–6232.
- 870 110 C. Czeslik and J. Jonas, *Chem Phys Lett*, 1999, **302**, 633–638.
- 871 111 M. Hu, J. Zhou, L. Jiang, Z. Wang, Y. Bao and S. Cui, *J Phys Chem B*, 2025, **129**, 4547–
872 4557.
- 873 112 C. W. Macosko, *Rheology: Principles, Measurements, and Applications*, Wiley-VCH,
874 New York, 1994.
- 875 113 S. K. Romberg and A. P. Kotula, *Addit Manuf*, 2023, **71**, 103589.
- 876 114 Y. Aota-Nakano, S. J. Li and M. Yamazaki, *Biochimica et Biophysica Acta (BBA) -*
877 *Biomembranes*, 1999, **1461**, 96–102.
- 878 115 S. J. Li, Y. Yamashita and M. Yamazaki, *Biophys J*, 2001, **81**, 983–993.
- 879 116 B. W. Muir, G. Zhen, P. Gunatillake and P. G. Hartley, *J Phys Chem B*, 2012, **116**, 3551–
880 3556.
- 881 117 A. S. Rafique, S. Khodaparast, A. S. Poulos, W. N. Sharratt, E. S. J. Robles and J. T.
882 Cabral, *Soft Matter*, 2020, **16**, 7835–7844.
- 883 118 L. Donina, A. Rafique, S. Khodaparast, L. Porcar and J. T. Cabral, *Soft Matter*, 2021, **17**,
884 10053–10062.
- 885 119 J. Nyvlt, O. Sohnel, M. Matuchova and M. Broul, *The Kinetics of industrial*
886 *crystallization*, Elsevier, Amsterdam, 1985.
- 887 120 B. C. Bhattarai, A. Parajuli and K. B. Stiansen-Snoerud, *Frontiers in Environmental*
888 *Engineering*, DOI:10.3389/fenv.2024.1519115.
- 889 121 C. Poelma, *Exp Fluids*, 2017, **58**, 3.
- 890 122 A. Talmon, E. Meshkati and F. van Rees, in *The 20th International Conference on*
891 *Transport and Sedimentation of Solid Particles. 50th anniversary*, Wydawnictwo
892 Uniwersytetu Przyrodniczego we Wrocławiu (WUELS Publishing House)), 2023, pp.
893 171–182.
- 894 123 S. Lerouge and J.-F. Berret, in *Advances in Polymer Science*, 2009, pp. 1–71.
- 895 124 T. Divoux, M. A. Fardin, S. Manneville and S. Lerouge, *Annu Rev Fluid Mech*, 2016, **48**,
896 81–103.



- 897 125 A. Abbasi Moud, J. Piette, M. Danesh, G. C. Georgiou and S. G. Hatzikiriakos, *J Rheol (N*
898 *YN Y)*, 2022, **66**, 79–90.
- 899 126 D. Kleinschmidt and V. Schöppner, *SPE Polymers*, 2023, **4**, 63–79.
- 900 127 M. Cloitre and R. T. Bonnecaze, *Rheol Acta*, 2017, **56**, 283–305.
- 901 128 A. Y. Malkin and S. A. Patlazhan, *Adv Colloid Interface Sci*, 2018, **257**, 42–57.
- 902 129 J. M. Seddon and R. H. Templer, in *Handbook of Biological Physics - Structure and*
903 *Dynamics of Membranes: From Cells to Vesicles*, eds. R. Lipowsky and R. Sackmann,
904 1995, vol. 1, pp. 97–160.
- 905 130 C. V. Kulkarni, *Nanoscale*, 2012, **4**, 5779.
- 906 131 A. Radaic, L. R. S. Barbosa, C. Jaime, Y. L. Kapila, F. B. T. Pessine and M. B. de Jesus,
907 in *Advances in Biomembranes and Lipid Self-Assembly*, 2016, vol. 24, pp. 1–42.
- 908 132 K. Steck, C. Schmidt and C. Stubenrauch, *Gels*, 2018, **4**, 78.
- 909 133 USPTO, US11028342B2, 2017.
- 910 134 X. Ma, Y. Duan and H. Li, *Powder Technol*, 2012, **230**, 127–133.
- 911 135 L. Chen, Y. Duan, C. Zhao and L. Yang, *Chemical Engineering and Processing: Process*
912 *Intensification*, 2009, **48**, 1241–1248.
- 913 136 E. J. Acosta, *Colloids Surf A Physicochem Eng Asp*, 2008, **320**, 193–204.
- 914 137 E. 'Acosta, J. 'Harwell and D. A. ' 'Sabatini, *Surfactant Formulation Engineering using*
915 *HLD and NAC*, Academic Press and AOCS Press, 1st edn., 2025.
- 916
- 917





SCHOOL OF MATERIALS ENGINEERING

Data Availability Statement

The data supporting this article have been plotted and included as part of the Supplementary Information.

Sincerely,

A handwritten signature in black ink that reads "Kendra A. Erk".

Kendra A. Erk, Ph.D.

Professor of Materials Engineering

erk@purdue.edu, 1-765-494-4118

Soft Matter Accepted Manuscript

